antibody and Alexa Fluor 647-conjugated anti-mouse IgG (H+L) antibody (Invitrogen). Images were acquired with a confocal microscope (LSM 700; Carl Zeiss). The enzymatic activity of calpains was measured using the Calpain-Glo Protease Assay (Promega) according to the manufacture's protocol.

Western Blot Analysis—Protein samples were fractionated with SDS-PAGE and transferred to PVDF membrane (GE Healthcare). The blotted membranes were incubated with primary antibodies followed by horseradish peroxidase-conjugated anti-mouse or anti-rabbit IgG antibody (Jackson ImmunoResearch Laboratories). Immunoreactive signals were detected with the ECL Plus Western blotting Detection System (GE Healthcare) and developed onto a film (Hyperfilm ECL; GE Healthcare Biosciences) or visualized using a lumino-image analyzer (ImageQuant LAS 4000 mini; GE Healthcare).

Primary Antibodies—The following antibodies were used: mouse monoclonal anti-N-cadherin antibody (clone 3B9, Invitrogen) raised against the intracellular domain of chicken N-cadherin, rabbit polyclonal anti-N-cadherin antibody (Santa Cruz Biotechnology, Inc.) raised against the extracellular domain of human N-cadherin, rabbit polyclonal anti-β-catenin antibody (Abcam), mouse monoclonal anti-Cx43 antibody (clone CX-1B1, Invitrogen), rabbit polyclonal anti-Cx43 antibody (Millipore), mouse monoclonal anti-sarcomeric α-actinin antibody (clone EA-53, Sigma), rabbit polyclonal anti-collagen 1 antibody (Abcam), mouse monoclonal anti-α-tubulin antibody (clone DM1A, Sigma), rabbit monoclonal anti-GAPDH antibody (clone 14C10, Cell Signaling Technology). A rabbit polyclonal antibody specific to the calpain cleavage site of the N-terminal 135-kDa fragment of αII-spectrin was described previously (25).

Real Time RT-PCR Analysis—Total RNA was extracted by using TRIzol reagent (Invitrogen), and single-stranded cDNA was transcribed by using QuantiTect Reverse Transcription kit (Qiagen) according to the manufacturer's protocol. We conducted quantitative real-time PCR analysis using Light Cycler TaqMan Master Kit (Roche Applied Science) with the target-specific primers and the matching probes designed by the Universal ProbeLibrary System (Roche Applied Science). Amplification conditions were initial denaturation for 10 min at 95 °C followed by 45 cycles of 10 s at 95 °C and 25 s at 60 °C. Individual PCR products were analyzed by melting point analysis. The expression level of a gene was normalized relative to that of *Gapdh* by using a comparative Ct method. The primer sequences and Universal Probe numbers were designed with the ProbeFinder software as following: *Nppa*, 5′-cacagatctgatggatttcaaga-3′ and 5′-cctcatcttctaccggcatc-3′, no. 25; *Nppb*, 5′-gtcagtcgtttgggctgtaac-3′ and 5′- agacccaggcagagtcagaa-3′, no. 71; *Acta1*, 5′-aatgagcgtttccgttgc-3′ and 5′-atccccgcagactccatac-3′, no. 94; *Gapdh*, 5′-tgtccgtcgtggatctgac-3′ and 5′-cctgcttcaccaccttcttg-3′, no. 80.

Statistics—The results are expressed as the mean ± S.E. Differences in measured values were analyzed using an unpaired 2-tailed Student's *t* test for two-group comparison and a 1-way analysis of variance followed by the Bonferroni's method for multi-group comparison. We estimated survival curves after MI by the Kaplan-Meier method and compared the two groups by the log-rank test. Values of $p < 0.05$ were considered statistically significant.

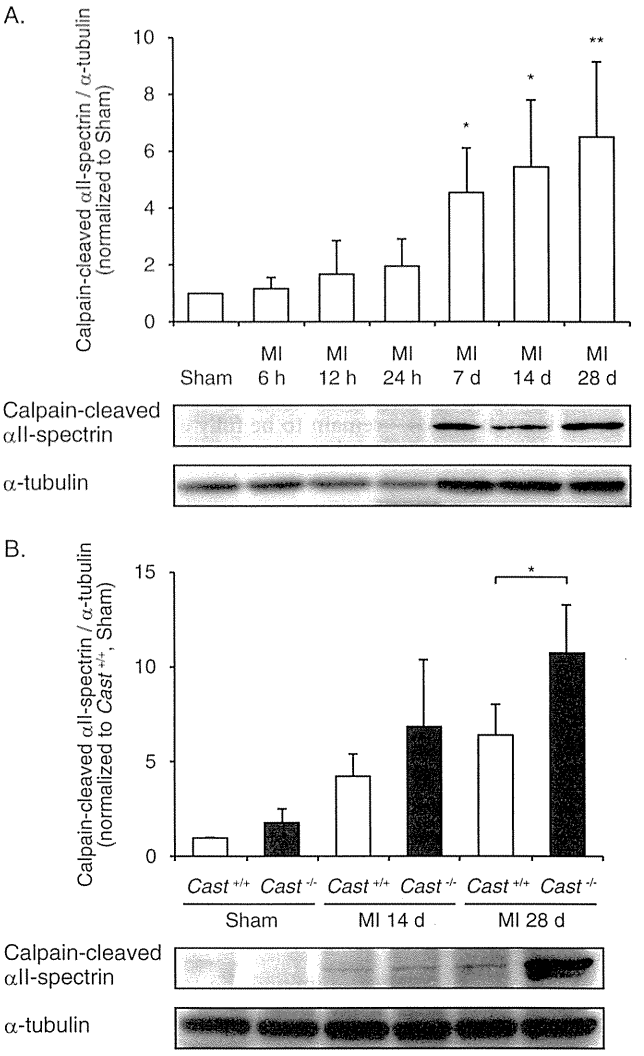

FIGURE 1. **Calpain activity in MI hearts of *Cast*$^{-/-}$ and *Cast*$^{+/+}$ mice.** *A*, time course of calpain activation after MI, determined by immunoblot analysis of calpain-cleaved αII-spectrin in the hearts of wild-type mice ($n = 5$). α-Tubulin was used as an internal control for the amount of loaded protein. The calpain-cleaved αII-spectrin/α-tubulin ratios were quantified by densitometry and plotted (*upper panel*). Data are presented as the mean ± S.E. *, $p < 0.05$; **, $p < 0.01$ *versus* Sham. *B*, comparison of calpain activation after MI between *Cast*$^{-/-}$ and *Cast*$^{+/+}$ mice ($n = 3 \sim 4$). The calpain-cleaved αII-spectrin/α-tubulin ratios were quantified by densitometry and plotted (*upper panel*). Data are presented as the mean ± S.E. *, $p < 0.05$.

RESULTS

Calpains Are Activated in the Chronic Phase but Not in the Acute Phase after MI—First, we examined the time course of change in calpain activity after MI in wild-type mice by using an antibody specific to the calpain-cleaved N-terminal 135-kDa fragment of αII-spectrin (25). Although it has been reported that intracellular Ca^{2+} is elevated immediately after myocardial ischemia (15), the level of spectrin proteolysis was unchanged within 24 h after MI (Fig. 1*A*). However, at 7 days after MI, spectrin proteolysis was significantly increased and sustained

TABLE 1

Basal heart rates, blood pressures, and echocardiographic parameters of *Cast*$^{-/-}$ and *Cast*$^{+/+}$ mice

Values are the mean ± S.E. LVEDD, left ventricular end-diastolic dimension; LVESD, left ventricular end-systolic dimension; IVSth, intraventricular septal thickness; PWth, left ventricular posterior wall thickness; FS, fractional shortening; HR, heart rate; SBP, systolic blood pressure; DBP, diastolic blood pressure; bpm, beats per min.

Parameters	*Cast*$^{+/+}$	*Cast*$^{-/-}$	*P*
Number	4	4	
Age (weeks)	8.60 ± 0.08	8.60 ± 0.20	0.54
Heart rate (bpm)	640 ± 13.6	646 ± 32.6	0.79
SBP (mm Hg)	98.9 ± 5.08	97.9 ± 5.73	0.79
DBP (mm Hg)	58.2 ± 4.26	52.6 ± 3.12	0.76
LVEDD (mm)	3.48 ± 0.03	3.46 ± 0.27	0.90
LVESD (mm)	1.71 ± 0.02	1.69 ± 0.04	0.51
IVSth (mm)	0.86 ± 0.11	0.89 ± 0.04	0.62
PWth (mm)	0.81 ± 0.07	0.90 ± 0.05	0.13
FS (%)	50.7 ± 1.28	50.9 ± 2.47	0.91

thereafter (Fig. 1*A*). These results suggest that calpains are activated not in the acute phase but in the subacute and chronic phase after MI.

Calpain Activation in the Chronic Phase after MI Is Enhanced in Cast$^{-/-}$ *Mice*—Next, we compared the activities of cardiac calpains after MI between *Cast*$^{-/-}$ and *Cast*$^{+/+}$ mice. It has been reported that basal activity of calpain is important for protein homeostasis in unstressed hearts (29), but the calpain activity in sham-operated hearts, as assessed by the level of spectrin proteolysis, was indistinguishable between *Cast*$^{-/-}$ and *Cast*$^{+/+}$ mice (Fig. 1*B*). Essentially, *Cast*$^{-/-}$ mice showed normal development, fertility, and life span (25). In addition, *Cast*$^{-/-}$ mice exhibited normal heart rates, blood pressures, and cardiac function under the physiological conditions as assessed by echocardiographic evaluation (Table 1). These results suggest that calpastatin deficiency has little effect on basal activity of calpain under the physiological conditions. However, as compared with *Cast*$^{+/+}$ mice, *Cast*$^{-/-}$ mice showed a significant increase in spectrin proteolysis at 28 days after MI (Fig. 1*B*), suggesting that calpastatin deficiency exaggerates activation of calpains when calpain activation is induced under stressed conditions.

LV Remodeling after MI Is Enhanced in Cast$^{-/-}$ *Mice*—At 14 days after MI, histological analysis with Masson's trichrome staining and echocardiographic examination revealed no significant difference in LV geometry and function between *Cast*$^{-/-}$ and *Cast*$^{+/+}$ mice (Fig. 2, *A* and *B*). However, at 28 days after MI, *Cast*$^{-/-}$ mice showed more severe LV dilatation and dysfunction than *Cast*$^{+/+}$ mice (Fig. 2, *C* and *D*). Because there was no significant difference in infarct size, determined either by area measurement or by length measurement, between *Cast*$^{-/-}$ and *Cast*$^{+/+}$ mice (Fig. 2, *E* and *F*), LV remodeling was promoted independently of the infarct size in *Cast*$^{-/-}$ mice. As a consequence, the survival rate was significantly lower in *Cast*$^{-/-}$ mice than in *Cast*$^{+/+}$ mice ($p < 0.05$), although the early death within 14 days after MI was comparable ($p = 0.058$) (Fig. 2*G*). These results suggest that enhanced activation of calpains in the chronic phase enhances LV remodeling in *Cast*$^{-/-}$ mice, leading to death possibly due to heart failure.

Myocardial Cell Death after MI Is Comparable between Cast$^{-/-}$ *and Cast*$^{+/+}$ *Mice*—Calpains have been implicated in the execution of cell death (1). Thus, we compared the prevalence of cardiomyocyte apoptosis in *Cast*$^{-/-}$ and *Cast*$^{+/+}$ mice by TUNEL staining. There was no significant difference in the number of TUNEL-positive cardiomyocytes in the infarct area of *Cast*$^{-/-}$ and *Cast*$^{+/+}$ hearts at 24 h after MI (Fig. 3, *A* and *B*). Throughout the period from 3 to 28 days, apoptotic cardiomyocytes were scarcely observed in the infarct or non-infarct area of both genotypes, and the number was not significantly different between *Cast*$^{-/-}$ and *Cast*$^{+/+}$ mice (Fig. 3, *C* and *D*). In addition, the infarct area of *Cast*$^{-/-}$ mice was not significantly different from that of *Cast*$^{+/+}$ mice at 28 days after MI (Fig. 2, *E* and *F*). These results suggest that calpastatin deficiency has little impact on myocardial cell death both in the acute phase and in the chronic phase after MI.

Calpain Activation Is Associated with a Decrease in N-cadherin Expression in the Border Zone of Cast$^{-/-}$ *Hearts*—To gain insights into the mechanism of how calpain activation leads to exacerbation of LV remodeling, we utilized immunofluorescence staining and assessed the cellular and subcellular localization of calpain activation in the infarct and border zones. In sham-operated hearts of *Cast*$^{+/+}$ mice, calpain-cleaved αII-spectrin was primarily localized in cardiomyocytes (Fig. 4*A*). Especially in cardiomyocytes, the fluorescence signals showed a characteristic cross-striated pattern that is typically seen with sarcomeric proteins, and intense fluorescence was colocalized with N-cadherin at the intercalated discs (Fig. 4*A*). A similar localization pattern of spectrin proteolysis with comparable intensity was observed in *Cast*$^{-/-}$ and *Cast*$^{+/+}$ mice (Fig. 4*A*). At 28 days after MI, the levels of calpain-cleaved αII-spectrin were indistinguishable in the non-infarct zone between *Cast*$^{-/-}$ and *Cast*$^{+/+}$ mice (Fig. 4*B*). However, we observed exaggeration of calpain-mediated spectrin proteolysis exclusively in cardiomyocytes at the border zone, adjacent to the infarct zone (Fig. 4*C*). *Cast*$^{-/-}$ mice showed significantly broader area of cardiomyocytes with intense immunofluorescence for calpain-cleaved αII-spectrin at the border zone than *Cast*$^{+/+}$ mice (Fig. 4, *C* and *D*). Notably, in cardiomyocytes at the border zone of *Cast*$^{-/-}$ mice, profound activation of calpains was associated with a considerable decrease in the expression of N-cadherin (Fig. 4*C*). N-cadherin is a Ca^{2+}-dependent transmembrane glycoprotein that enhances cell adhesion by binding to α-, β-, and γ-catenins at adherens junction (30) and stabilizes gap junction formation by maintaining connexin 43 (Cx43) at intercalated discs (31). In parallel with the decrease in N-cadherin expression, the expression levels of β-catenin and Cx43 were decreased in cardiomyocytes at the border zone of *Cast*$^{-/-}$ mice (Fig. 4, *E* and *F*). Next, we isolated RNA from the border zone of MI hearts for quantification of the expression levels of fetal cardiac genes. *Cast*$^{-/-}$ mice showed a significant increase in the expressions of *Nppa*, *Nppb*, and *Acta1* as compared with *Cast*$^{+/+}$ mice (Fig. 5*A*). Furthermore, immunohistochemical analysis revealed that the expression of collagen 1 was significantly increased in the border zone of *Cast*$^{-/-}$ mice as compared with *Cast*$^{+/+}$ mice (Fig. 5*B*). These results suggest that molecular and cellular remodeling in the border zone was more prominent in *Cast*$^{-/-}$ mice than in *Cast*$^{+/+}$ mice. Collectively, we speculate that unregulated activation of calpains in cardiomyocytes may disassemble the cadherin-mediated structures of adherens junction and gap junction of cardiomyocytes

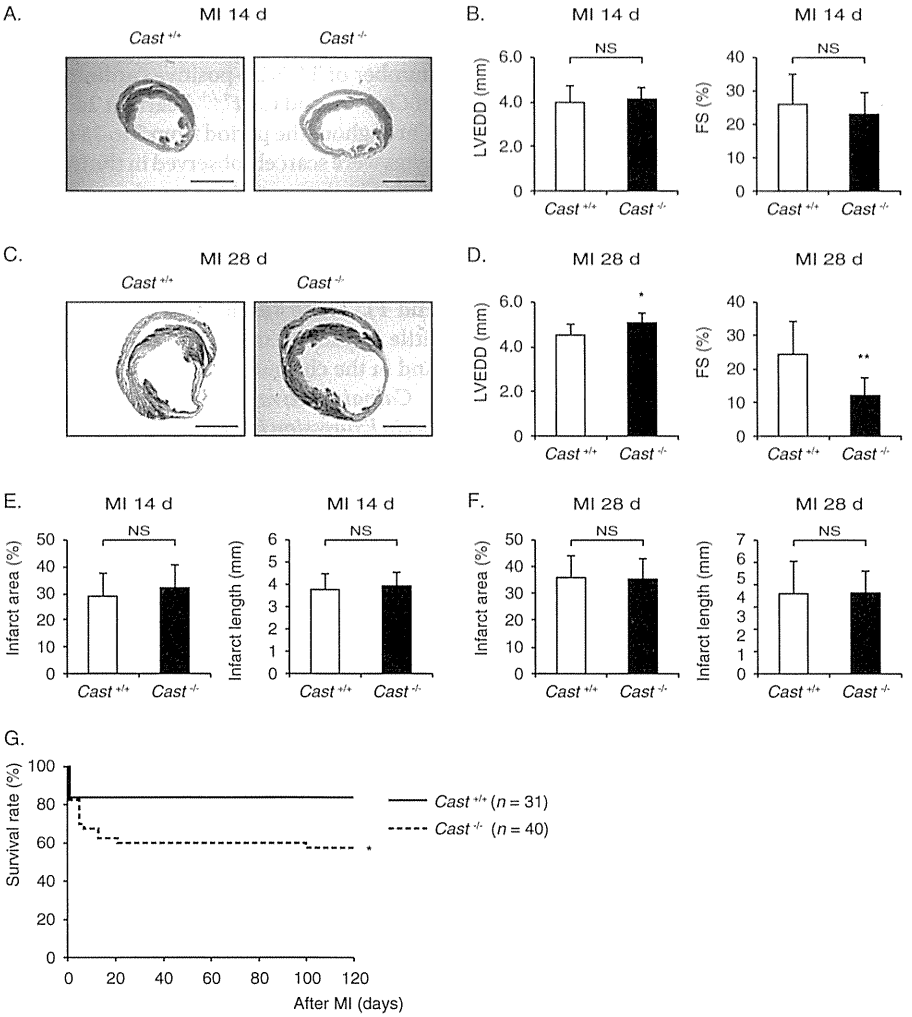

FIGURE 2. **LV remodeling after MI in *Cast*$^{-/-}$ and *Cast*$^{+/+}$ mice.** *A*, Masson's trichrome staining of *Cast*$^{-/-}$ and *Cast*$^{+/+}$ hearts at 14 days after MI. *Scale bars*, 2 mm. *B*, echocardiographic parameters of *Cast*$^{-/-}$ and *Cast*$^{+/+}$ mice at 14 days after MI. *C*, Masson's trichrome staining of *Cast*$^{-/-}$ and *Cast*$^{+/+}$ hearts at 28 days after MI. *Scale bars*, 2 mm. *D*, echocardiographic parameters of *Cast*$^{-/-}$ and *Cast*$^{+/+}$ mice at 28 days after MI. *E* and *F*, infarct area (*light panels*) and infarct length (*right panels*) of *Cast*$^{-/-}$ and *Cast*$^{+/+}$ hearts at 14 days (*E*) and 28 days (*F*) after MI. *G*, Kaplan-Meier survival curves of *Cast*$^{+/+}$ ($n = 31$) and *Cast*$^{-/-}$ mice ($n = 40$) after MI. *LVEDD*, LV end-diastolic dimension; *FS*, fractional shortening. Values represent the mean ± S.E. of data from 10 mice in each group. *NS*, not significant. *, $p < 0.05$; **, $p < 0.01$ *versus* *Cast*$^{+/+}$ mice.

in the border zone and thereby lead to progression of LV remodeling after MI.

Calpain Activation Causes N-cadherin Cleavage and Disassembles Cadherin-based Cell Adhesions in Cultured Cardiomyocytes of Neonatal Rats—To examine whether calpain activation was sufficient for disruption of N-cadherin-based cell adhesions, we stimulated cultured cardiomyocytes of neonatal rats with the Ca^{2+} ionophore ionomycin. Direct measurement of the enzymatic activity of calpains using a luminescent assay revealed that calpain enzymatic activity was significantly enhanced after stimulation with ionomycin, which was significantly, but not completely, repressed by pretreatment with the cell-permeable calpain inhibitor MDL28170 (Fig. 6*A*). Western blot analysis showed that the expression levels of full-length N-cadherin (140 kDa) were significantly decreased by stimulation with ionomycin, which was attenuated by pretreatment with MDL28170 (Fig. 6, *B* and *C*). In parallel with a decrease in the levels of full-length N-cadherin, ionomycin significantly increased the generation of the 106- and 37-kDa fragments, as detected by anti-N-cadherin antibodies raised against the N-terminal extracellular domain and the C-terminal intracellular domain, respectively (Fig. 6*B*). Similarly, the expression levels of β-catenin and Cx43 were significantly decreased by stimulation with ionomycin, which was attenuated by pretreatment with MDL28170 (Fig. 6, *B* and *C*).

Confocal immunocytochemistry revealed reduction in the expression levels of N-cadherin and β-catenin at the intercalated discs when cardiomyocytes were stimulated with ionomycin (Fig. 7*A*). Meanwhile, Cx43 immunofluorescent signals showed reduction at the intercalated discs and concomitant intracellular redistribution in response to ionomycin stimulation (Fig. 7*B*). Ionomycin-induced effects on the amount and spatial distribution of these intercalated disc proteins were prevented by pretreatment with MDL28170 (Fig. 7, *A* and *B*). These results suggest that calpain activation is sufficient to cause degradation of N-cadherin and to dis-

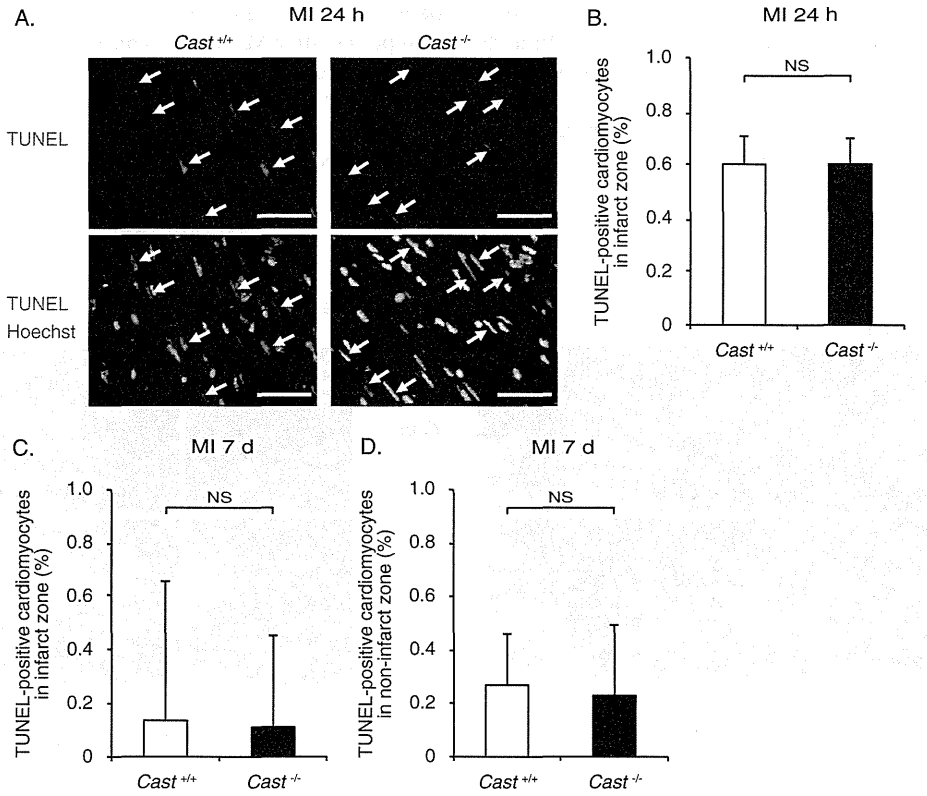

FIGURE 3. **Cardiomyocyte apoptosis after MI in *Cast*$^{-/-}$ and *Cast*$^{+/+}$ mice.** *A*, TUNEL staining with nuclear staining with Hoechst 33258 in the infarct zone of *Cast*$^{-/-}$ and *Cast*$^{+/+}$ mice at 24 h after MI. *Scale bars*, 50 μm. *B*, percentage of TUNEL-positive cardiomyocytes in the infarct zone of *Cast*$^{-/-}$ and *Cast*$^{+/+}$ mice at 24 h after MI was calculated. Values represent the mean ± S.E. (500 cardiomyocytes sampled from 12 visual fields from 3 mice in each group). *NS*, not significant. *C* and *D*, percentage of TUNEL-positive cardiomyocytes in the infarct zone (*C*) and non-infarct zone (*D*) of *Cast*$^{-/-}$ and *Cast*$^{+/+}$ mice at 7 days after MI was calculated. Values represent the mean ± S.E. (800 cardiomyocytes sampled from 12 visual fields from 3 mice in each group). *NS*, not significant.

assemble cadherin-based cell adhesions in rat neonatal cardiomyocytes.

DISCUSSION

In the present study we provided experimental evidence that calpains impaired the cell-cell interactions through degradation of cadherin-associated protein complex and thereby promoted LV remodeling after MI. Calpain-mediated proteolysis was increased in the chronic phase (7 days and later), not in the acute phase (before 24 h), after MI, and profound activation of calpains exacerbated LV remodeling without affecting myocardial cell death in *Cast*$^{-/-}$ mice. In the border zone of MI hearts, *Cast*$^{-/-}$ mice showed a decrease in N-cadherin expression concomitant with an increase in calpain activation and prominent myocardial remodeling. In cultured cardiomyocytes calpain activation caused degradation of N-cadherin and disorganization of cadherin-based cell adhesions.

The pathogenic role of calpains in MI hearts has remained unclear despite the efforts of many laboratories. One of the major obstacles for the study of calpains has been the lack of reliable methods to measure calpain activity accurately *in vivo*. Previous reports demonstrated that expression levels or enzymatic activities of calpains were increased in the hearts after MI (17–21), but these results must be interpreted cautiously. Obviously, the protein content of calpains does not necessary correlate with their proteolytic activity, and the *in vitro* enzymatic assays using homogenized tissue samples after the addition of Ca^{2+} merely indicate the proteolytic capacity of calpains, not the calpain activity *in situ*. However, in our study the use of a specific antibody against calpain-cleaved fragment of αII-spectrin has allowed for direct observation of the proteolytic activity of calpains in *in vivo* hearts in temporal and spatial terms. Another obstacle has been the lack of specific and effective calpain inhibitors (1). The best approach for identifying the role of calpains in cellular function is to introduce calpastatin, the specific and endogenous inhibitor of calpains. However, according to a recent study, cardiac overexpression of calpastatin inhibited basal calpain activity and resulted in spontaneous and progressive heart failure (29). Thus, we have analyzed *Cast*$^{-/-}$ and *Cast*$^{+/+}$ mice to examine the consequences of exaggerated calpain activation in the hearts after MI.

In a variety of mammalian cells, activated calpains mediate cell death by multiple mechanisms. For example, calpains activate p53 (32), and pro-apoptotic BH3-only protein Bax (33) and Bid (34) inactivate anti-apoptotic Bcl-xL (35), facilitate the release of apoptosis-inducing factor (AIF) from mitochondria (36, 37), induce caspase-12 activation (35) and release of lysosomal cathepsins (38), cleave autophagy regulating protein Atg5 (39), degrade cytoskeletal proteins (40), disrupt ion homeostasis (9, 40, 41), and increase plasma membrane permeability (40). *In vivo* transgenic overexpression of calpain 1 in the heart

has induced heart failure, which is associated with cardiomyocyte necrosis and mononuclear cell infiltration (29). In addition, profound calpain activation in *Cast*$^{-/-}$ mice has exacerbated excitotoxicity by kainite, leading to neuronal DNA fragmentation in the brain (25). However, the prevalence of cardiomyocyte apoptosis and the infarct size did not differ between *Cast*$^{-/-}$ and *Cast*$^{+/+}$ mice throughout the observation period after MI (Figs. 2 and 3). These results suggest that calpastatin deficiency has little effect on myocardial cell death in MI hearts. Previous reports demonstrated that pharmacological inhibition of calpains reduced the infarct size (22, 23). In addition, recent reports showed that overexpression of *Capn1*

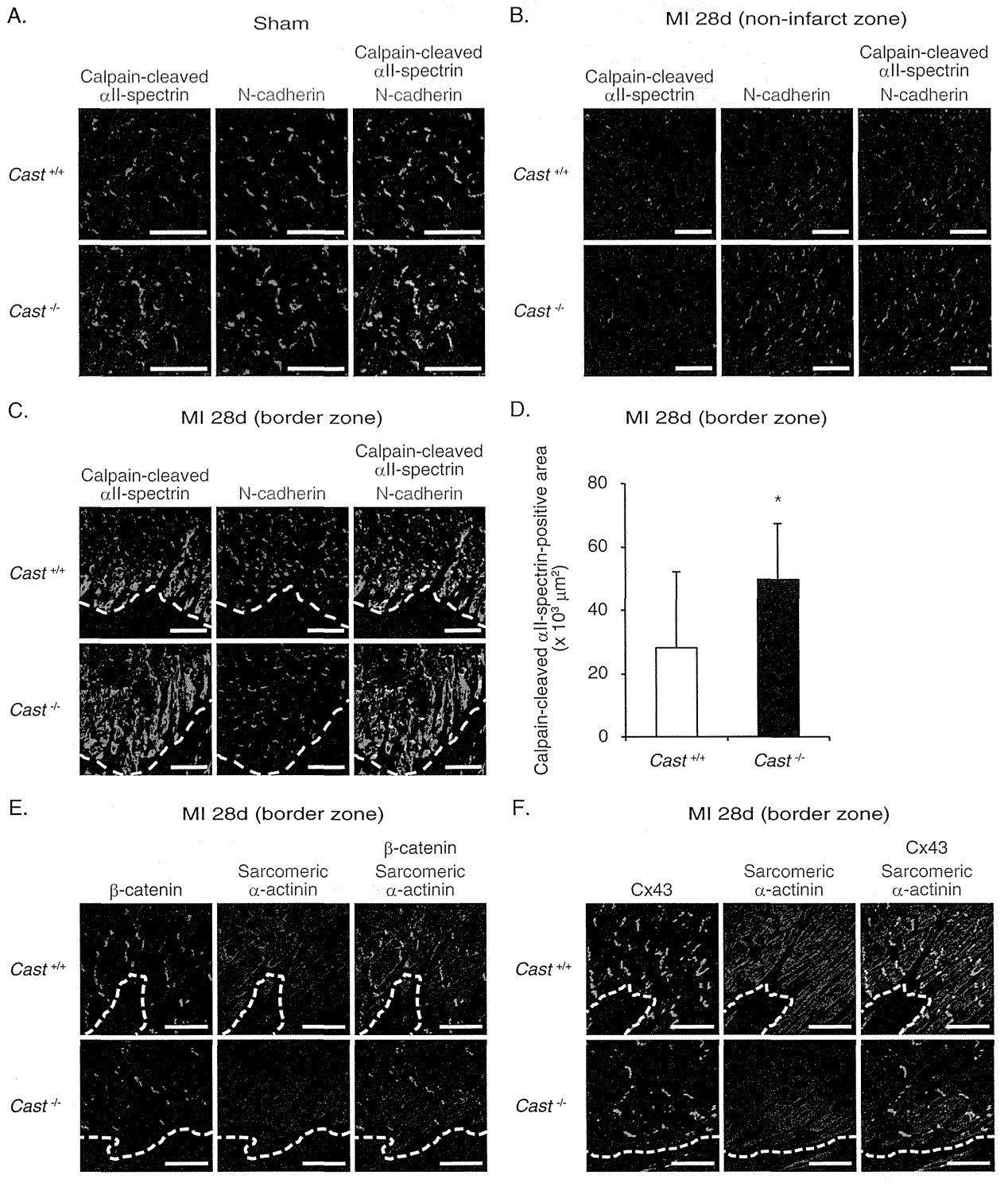

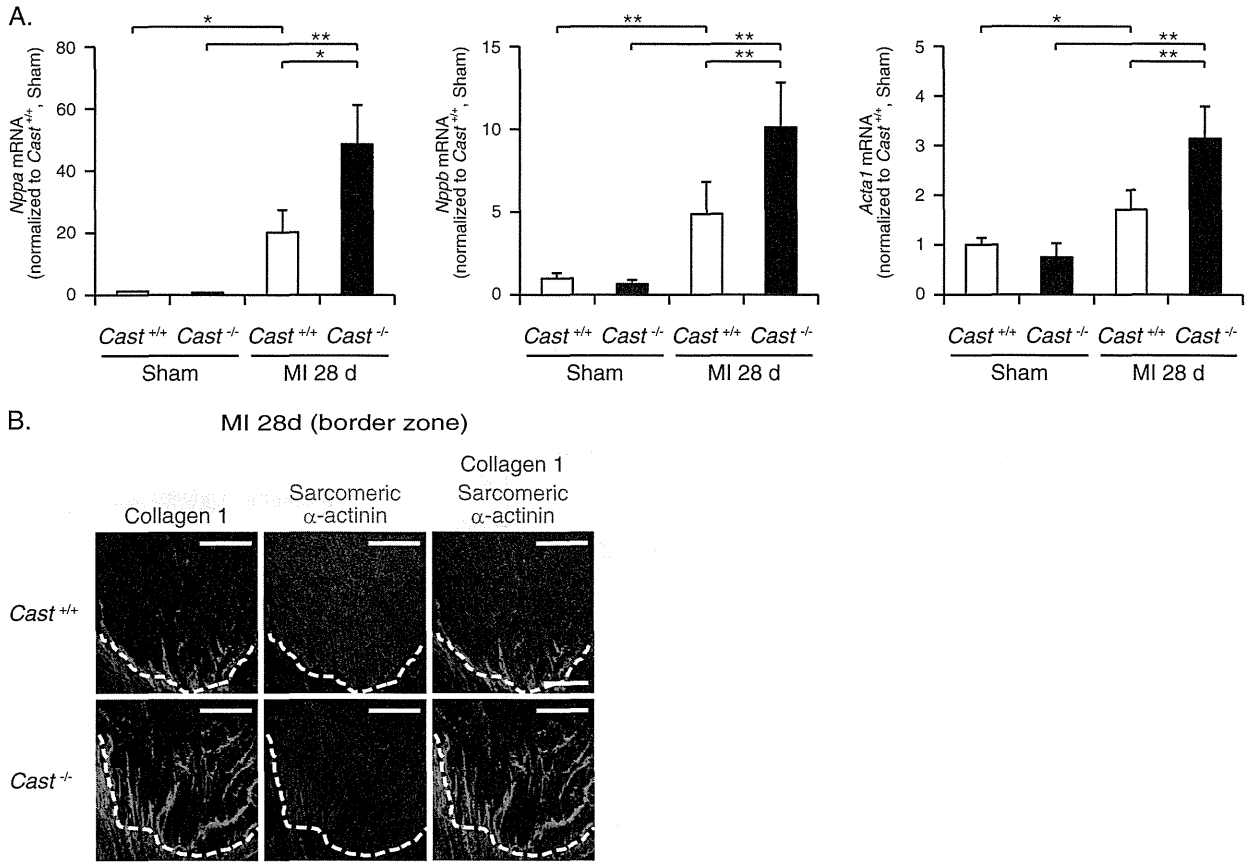

FIGURE 5. **Molecular and histological changes in the border zone of $Cast^{-/-}$ and $Cast^{+/+}$ hearts after MI.** *A*, the mRNA expressions of *Nppa*, *Nppb*, and *Acta1* in the border zone of $Cast^{-/-}$ and $Cast^{+/+}$ hearts at 28 days after MI and in sham-operated $Cast^{-/-}$ and $Cast^{+/+}$ hearts ($n = 3 \sim 5$, in each group). Values represent the mean ± S.E. *, $p < 0.05$; **, $p < 0.01$ *versus* sham-operated $Cast^{+/+}$ mice. *B*, immunofluorescence of the border zone in $Cast^{-/-}$ and $Cast^{+/+}$ hearts at 28 days after MI ($n = 5$, in each group). Collagen 1 and sarcomeric α-actinin are represented in *green* and *red*, respectively. *Scale bars*, 200 μm. The *dotted lines* indicate the boundary between the border zone where viable cardiomyocytes remain (*above the dotted line*) and the infarct zone (*below the dotted line*).

increased infarct size and enhanced myocardial cell death after MI (10), whereas genetic disruption of *Capn1* or *Capns1* provided the reciprocal results (10, 42). However, cardiac-specific *Capns1* knock-out mice were susceptible for hemodynamic stress-induced myocardial injury because of defective membrane repair, indicating that calpains play a beneficial role as well (43). Because calpain activity in sham-operated hearts was indistinguishable between $Cast^{-/-}$ and $Cast^{+/+}$ hearts (Fig. 1*B*), our study presented experimental evidence that inhibition of calpain activation without affecting the basal activity had little impact on myocardial cell death after MI.

Temporal and spatial analyses of calpain-cleaved αII-spectrin revealed that calpain activation was induced at the border zone of MI hearts in the chronic phase (Fig. 4*C*). After MI, the border zone expands in response to increased wall stress, promoting further LV dilatation and contractile dysfunction (44). Because calpain activation was followed by progressive contractile dysfunction and LV dilatation (Figs. 1 and 2), we speculate that profound activation of calpains at the border zone may contribute to exacerbation of LV remodeling in $Cast^{-/-}$ mice. According to *in vitro* assays, activated calpains cleave a large number of proteins including cytoskeletal proteins, membrane-associated proteins, signaling mediators, and transcription factors (1). Recent reports showed that calpain activation induced IκB degradation and NF-κB activation (45) and that disruption of *Capns1* inhibited NF-κB signaling and inflamma-

FIGURE 4. **Cellular and subcellular localization of calpain activation in the border zone of $Cast^{-/-}$ and $Cast^{+/+}$ hearts after MI.** *A*, immunofluorescence of sham-operated $Cast^{-/-}$ and $Cast^{+/+}$ hearts ($n = 5$, in each group). Calpain-cleaved αII-spectrin and N-cadherin are represented in *green* and *red*, respectively. Co-localization of calpain-cleaved αII-spectrin and N-cadherin at the intercalated discs is indicated by the *yellow merging of the green and red labels*. *Scale bars*, 50 μm. *B*, immunofluorescence of the non-infarct zone in $Cast^{-/-}$ and $Cast^{+/+}$ hearts at 28 days after MI. Calpain-cleaved αII-spectrin and N-cadherin are represented in *green* and *red*, respectively. *Scale bars*, 100 μm. *C*, immunofluorescence of the border zone in $Cast^{-/-}$ and $Cast^{+/+}$ hearts at 28 days after MI ($n = 5$, in each group). Calpain-cleaved αII-spectrin and N-cadherin are represented in *green* and *red*, respectively. *Scale bars*, 100 μm. *D*, calculated areas of cardiomyocytes with intense immunofluorescence for calpain-cleaved αII-spectrin at the border zone in $Cast^{-/-}$ and $Cast^{+/+}$ hearts at 28 days after MI ($n = 5$, in each group). Data are presented as the mean ± S.E. *, $p < 0.05$. *E*, immunofluorescence of the border zone in $Cast^{-/-}$ and $Cast^{+/+}$ hearts at 28 days after MI ($n = 5$, in each group). β-Catenin and sarcomeric α-actinin are represented in *green* and *red*, respectively. *Scale bars*, 100 μm. *F*, immunofluorescence of the border zone in $Cast^{-/-}$ and $Cast^{+/+}$ hearts at 28 days after MI ($n = 5$, in each group). Cx43 and sarcomeric α-actinin are represented in *green* and *red*, respectively. *Scale bars*, 100 μm. The *dotted lines* (*C*, *E*, and *F*) indicate the boundary between the border zone where viable cardiomyocytes remain (*above the dotted line*) and the infarct zone (*below the dotted line*).

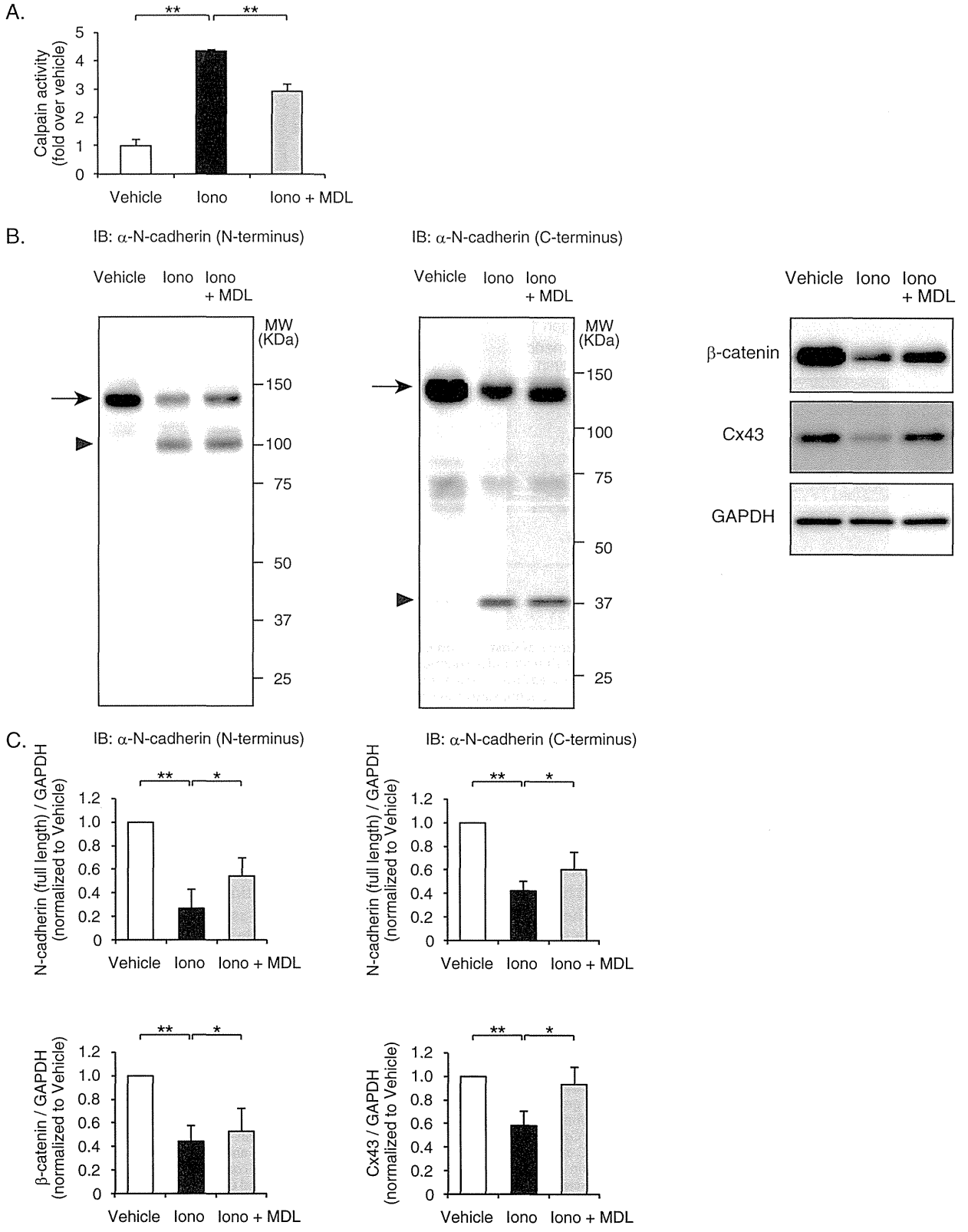

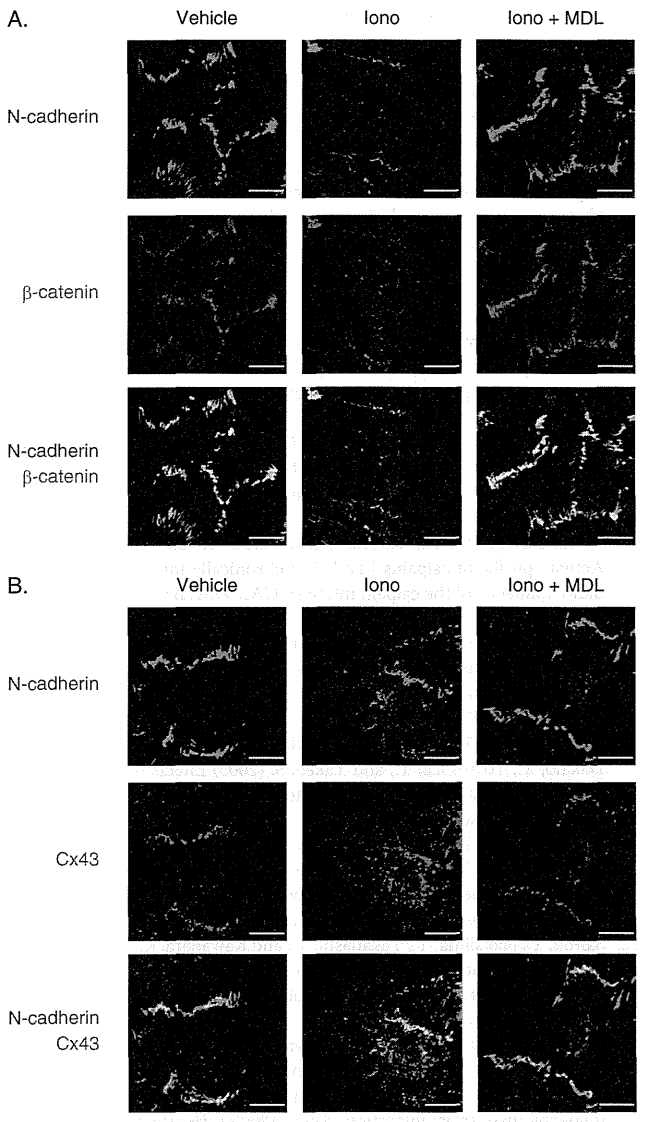

FIGURE 7. **Calpain-mediated disassembly of intercalated disc proteins in rat neonatal cardiomyocytes.** *A*, immunofluorescence of N-cadherin and β-catenin in rat neonatal cardiomyocytes. Cells were pretreated with MDL28170 (*MDL*, 10 μM) and stimulated with ionomycin (*Iono*, 10 μM) for 10 min. N-cadherin and β-catenin are represented in *green* and *red*, respectively. Experiments were repeated three times in triplicate, and the representative images are shown. *Scale bars*, 10 μm. *B*, immunofluorescence of N-cadherin and Cx43 in rat neonatal cardiomyocytes. Cells were pretreated with MDL28170 (10 μM) and stimulated with ionomycin (10 μM) for 10 min. N-cadherin and Cx43 are represented in *green* and *red*, respectively. Experiments were repeated three times in triplicate, and the representative images are shown. *Scale bars*, 10 μm.

tion, leading to improvement of LV remodeling after MI (42). In an attempt to explore potential calpain substrates in MI hearts, we found that calpain-cleaved αII-spectrin was co-localized with N-cadherin at the intercalated discs (Fig. 4, *A–C*). Importantly, increased calpain proteolysis was associated with a decrease in N-cadherin expression in cardiomyocytes at the border zone of $Cast^{-/-}$ hearts (Fig. 4*C*). In cultured cardiomyocytes, N-cadherin was cleaved in the presence of ionomycin, resulting in the generation of at least two fragments, an N-terminal 106-kDa and a C-terminal 37-kDa fragment. A calpain inhibitor MDL28170 significantly but not completely suppressed ionomycin-stimulated activation of calpains (Fig. 6*A*) and thereby prevented a significant degree of N-cadherin cleavage (Fig. 6*B*). In contrast to the degradation of full-length N-cadherin, the generation of cleaved fragments was not repressed by pretreatment with the calpain inhibitor (Fig. 6*B*). We speculate that the cleaved fragments may become unstable and susceptible to further degradation by undefined proteases. Previous reports demonstrated that calpains cleaved at least four regions of the intracellular domain of N-cadherin in neural cells (46, 47) and that calpain-mediated N-cadherin cleavage suppressed cell-cell adhesion in myogenic C2C12 cells (47). In cultured cardiomyocytes, calpain activation by ionomycin disassembled cadherin-based cell-cell adhesion consisting of intercalated disc proteins such as β-catenin and Cx43 (Fig. 7). It was reported that targeted disruption of N-cadherin in the hearts caused disassembly of intercalated discs, leading to LV dilatation and dysfunction (48). In addition, abnormal mechanical coupling through intercalated discs has been observed in the hearts of animal model and human patients with heart failure (49–51). Therefore, we assume that calpain activation-associated down-regulation of N-cadherin at the border zone is profoundly involved in the progression of LV remodeling after MI. It has been reported that a large number of proteins are cleaved by calpains in *in vitro* assays, including cytoskeletal proteins, membrane-associated proteins, kinases and phosphatases, and transcription factors (1). To prove the pathogenic significance of calpain-mediated cleavage of N-cadherin, our observation must be further investigated in future studies using knock-in mice of N-cadherin that is resistant to calpain cleavage for testing if these mice would rescue the exacerbated LV remodeling after MI in $Cast^{-/-}$ mice.

It remains an open question of what triggers calpain activation at the border zone cardiomyocytes in the chronic phase after MI. One of the candidates upstream of calpain activation is the renin-angiotensin system. It is well established that the local renin-angiotensin system is activated during the remodeling process after MI and that pharmacological or genetic blockade of renin-angiotensin system prevented LV remodeling after MI in many animal models and human patients (52). In cultured vascular smooth muscle cells, stimulation with angiotensin II (Ang II) has increased the calpain activity through transactivation of epidermal growth factor receptor and systemic overexpression of calpastatin blunted cardiac hypertro-

FIGURE 6. **Calpain-mediated degradation of N-cadherin and down-regulation of intercalated disc proteins in rat neonatal cardiomyocytes.** *A*, ionomycin-induced calpain activation in rat neonatal cardiomyocytes. Cells were pretreated with MDL28170 (10 μM) and stimulated with ionomycin (10 μM) for 10 min, and calpain activity was determined by a luminescent assay. Experiments were repeated three times in triplicate, and data are shown as -fold induction over vehicle control (mean ± S.E.). *Iono*, ionomycin; *MDL*, MDL28170. **, $p < 0.01$. *B*, immunoblot (*IB*) analysis of N-cadherin, β-catenin, and Cx43 in rat neonatal cardiomyocytes. Besides the full-length N-cadherin (*arrows*), the degraded N-terminal fragments (*arrowhead*) and C-terminal fragments (*arrowhead*) were detected by anti-N-cadherin antibody raised against the extracellular domain and intracellular domain of N-cadherin, respectively. *C*, quantitation of the N-cadherin (N terminus)/GAPDH ($n = 6$), N-cadherin (C terminus)/GAPDH ($n = 7$), β-catenin/GAPDH ($n = 3$), and Cx43/GAPDH ($n = 4$) are shown as *bar graphs* (*right panel*). Data are presented as the mean ± S.E. *, $p < 0.05$; **, $p < 0.01$.

phy and perivascular inflammation in Ang II-infused mice (53). A recent study showed that calpain activation mediated Ang II-induced endothelial dysfunction in rodents (54). It is intriguing that activation of Ang II receptor signaling by locally produced Ang II and mechanical stress (28) may lead to calpain activation and thereby promote LV remodeling after MI. Even so, we have to assume that additional undefined factors play a regulatory role in activating calpains in a temporally and spatially restricted manner in MI hearts.

In conclusion, calpains are activated in the chronic phase after MI, and profound activation of calpains may exacerbate LV remodeling possibly through the alterations of intercalated disc organization in cardiomyocytes at the border zone. Therefore, pharmacological intervention of the calpain-calpastatin system may emerge as a promising strategy in the treatment of LV remodeling after MI unless it hampers the basal calpain activity.

Acknowledgments—We thank A. Furuyama, M. Ikeda, Y. Ohtsuki, I. Sakamoto, M. Shimizu, K. Kawaguchi, N. Miyagawa, H. Taniwaki, and Y. Ueda for excellent technical assistance.

REFERENCES

1. Goll, D. E., Thompson, V. F., Li, H., Wei, W., and Cong, J. (2003) The calpain system. *Physiol. Rev.* **83,** 731–801
2. Hanna, R. A., Campbell, R. L., and Davies, P. L. (2008) Calcium-bound structure of calpain and its mechanism of inhibition by calpastatin. *Nature* **456,** 409–412
3. Zatz, M., and Starling, A. (2005) Calpains and disease. *N. Engl. J. Med.* **352,** 2413–2423
4. Murphy, E., and Steenbergen, C. (2008) Mechanisms underlying acute protection from cardiac ischemia-reperfusion injury. *Physiol. Rev.* **88,** 581–609
5. Matsumura, Y., Saeki, E., Inoue, M., Hori, M., Kamada, T., and Kusuoka, H. (1996) Inhomogeneous disappearance of myofilament-related cytoskeletal proteins in stunned myocardium of guinea pig. *Circ. Res.* **79,** 447–454
6. Gao, W. D., Atar, D., Liu, Y., Perez, N. G., Murphy, A. M., and Marban, E. (1997) Role of troponin I proteolysis in the pathogenesis of stunned myocardium. *Circ. Res.* **80,** 393–399
7. Papp, Z., van der Velden, J., and Stienen, G. J. (2000) Calpain-I induced alterations in the cytoskeletal structure and impaired mechanical properties of single myocytes of rat heart. *Cardiovasc. Res.* **45,** 981–993
8. Tsuji, T., Ohga, Y., Yoshikawa, Y., Sakata, S., Abe, T., Tabayashi, N., Kobayashi, S., Kohzuki, H., Yoshida, K. I., Suga, H., Kitamura, S., Taniguchi, S., and Takaki, M. (2001) Rat cardiac contractile dysfunction induced by Ca^{2+} overload: possible link to the proteolysis of α-fodrin. *Am. J. Physiol. Heart Circ. Physiol.* **281,** H1286–H1294
9. Inserte, J., Garcia-Dorado, D., Hernando, V., and Soler-Soler, J. (2005) Calpain-mediated impairment of Na^+/K^+-ATPase activity during early reperfusion contributes to cell death after myocardial ischemia. *Circ. Res.* **97,** 465–473
10. Kang, M. Y., Zhang, Y., Matkovich, S. J., Diwan, A., Chishti, A. H., and Dorn, G. W., 2nd (2010) Receptor-independent cardiac protein kinase Cα activation by calpain-mediated truncation of regulatory domains. *Circ. Res.* **107,** 903–912
11. Neuhof, C., Fabiunke, V., Deibele, K., Speth, M., Möller, A., Lubisch, W., Fritz, H., Tillmanns, H., and Neuhof, H. (2004) Reduction of myocardial infarction by calpain inhibitors A-705239 and A-705253 in isolated perfused rabbit hearts. *Biol. Chem.* **385,** 1077–1082
12. Khalil, P. N., Neuhof, C., Huss, R., Pollhammer, M., Khalil, M. N., Neuhof, H., Fritz, H., and Siebeck, M. (2005) Calpain inhibition reduces infarct size and improves global hemodynamics and left ventricular contractility in a porcine myocardial ischemia/reperfusion model. *Eur. J. Pharmacol.* **528,** 124–131
13. Yoshikawa, Y., Hagihara, H., Ohga, Y., Nakajima-Takenaka, C., Murata, K. Y., Taniguchi, S., and Takaki, M. (2005) Calpain inhibitor-1 protects the rat heart from ischemia-reperfusion injury: analysis by mechanical work and energetics. *Am. J. Physiol. Heart Circ. Physiol.* **288,** H1690–H1698
14. Hernando, V., Inserte, J., Sartório, C. L., Parra, V. M., Poncelas-Nozal, M., and Garcia-Dorado, D. (2010) Calpain translocation and activation as pharmacological targets during myocardial ischemia/reperfusion. *J. Mol. Cell Cardiol.* **49,** 271–279
15. Steenbergen, C., Murphy, E., Levy, L., and London, R. E. (1987) Elevation in cytosolic free calcium concentration early in myocardial ischemia in perfused rat heart. *Circ. Res.* **60,** 700–707
16. Imahashi, K., Pott, C., Goldhaber, J. I., Steenbergen, C., Philipson, K. D., and Murphy, E. (2005) Cardiac-specific ablation of the Na^+-Ca^{2+} exchanger confers protection against ischemia/reperfusion injury. *Circ. Res.* **97,** 916–921
17. Sandmann, S., Yu, M., and Unger, T. (2001) Transcriptional and translational regulation of calpain in the rat heart after myocardial infarction: effects of AT(1) and AT(2) receptor antagonists and ACE inhibitor. *Br. J. Pharmacol.* **132,** 767–777
18. Sandmann, S., Prenzel, F., Shaw, L., Schauer, R., and Unger, T. (2002) Activity profile of calpains I and II in chronically infarcted rat myocardium: influence of the calpain inhibitor CAL 9961. *Br. J. Pharmacol.* **135,** 1951–1958
19. Yoshida, H., Takahashi, M., Koshimizu, M., Tanonaka, K., Oikawa, R., Toyo-oka, T., and Takeo, S. (2003) Decrease in sarcoglycans and dystrophin in failing heart following acute myocardial infarction. *Cardiovasc. Res.* **59,** 419–427
20. Takahashi, M., Tanonaka, K., Yoshida, H., Oikawa, R., Koshimizu, M., Daicho, T., Toyo-Oka, T., and Takeo, S. (2005) Effects of ACE inhibitor and AT1 blocker on dystrophin-related proteins and calpain in failing heart. *Cardiovasc. Res.* **65,** 356–365
21. Takahashi, M., Tanonaka, K., Yoshida, H., Koshimizu, M., Daicho, T., Oikawa, R., and Takeo, S. (2006) Possible involvement of calpain activation in pathogenesis of chronic heart failure after acute myocardial infarction. *J. Cardiovasc. Pharmacol.* **47,** 413–421
22. Saitoh, T., Nakajima, T., Takahashi, T., and Kawahara, K. (2006) Changes in cardiovascular function on treatment of inhibitors of apoptotic signal transduction pathways in left ventricular remodeling after myocardial infarction. *Cardiovasc. Pathol.* **15,** 130–138
23. Mani, S. K., Balasubramanian, S., Zavadzkas, J. A., Jeffords, L. B., Rivers, W. T., Zile, M. R., Mukherjee, R., Spinale, F. G., and Kuppuswamy, D. (2009) Calpain inhibition preserves myocardial structure and function following myocardial infarction. *Am. J. Physiol. Heart Circ. Physiol.* **297,** H1744–H1751
24. Carragher, N. O. (2006) Calpain inhibition: a therapeutic strategy targeting multiple disease states. *Curr. Pharm. Des.* **12,** 615–638
25. Takano, J., Tomioka, M., Tsubuki, S., Higuchi, M., Iwata, N., Itohara, S., Maki, M., and Saido, T. C. (2005) Calpain mediates excitotoxic DNA fragmentation via mitochondrial pathways in adult brains: evidence from calpastatin mutant mice. *J. Biol. Chem.* **280,** 16175–16184
26. Kawai, S., Takagi, Y., Kaneko, S., and Kurosawa, T. (2011) Effect of three types of mixed anesthetic agents alternate to ketamine in mice. *Exp. Anim.* **60,** 481–487
27. Takagawa, J., Zhang, Y., Wong, M. L., Sievers, R. E., Kapasi, N. K., Wang, Y., Yeghiazarians, Y., Lee, R. J., Grossman, W., and Springer, M. L. (2007) Myocardial infarct size measurement in the mouse chronic infarction model: comparison of area- and length-based approaches. *J. Appl. Physiol.* **102,** 2104–2111
28. Zou, Y., Akazawa, H., Qin, Y., Sano, M., Takano, H., Minamino, T., Makita, N., Iwanaga, K., Zhu, W., Kudoh, S., Toko, H., Tamura, K., Kihara, M., Nagai, T., Fukamizu, A., Umemura, S., Iiri, T., Fujita, T., and Komuro, I. (2004) Mechanical stress activates angiotensin II type 1 receptor without the involvement of angiotensin II. *Nat. Cell Biol.* **6,** 499–506
29. Galvez, A. S., Diwan, A., Odley, A. M., Hahn, H. S., Osinska, H., Melendez, J. G., Robbins, J., Lynch, R. A., Marreez, Y., and Dorn, G. W., 2nd. (2007) Cardiomyocyte degeneration with calpain deficiency reveals a critical role

in protein homeostasis. *Circ. Res.* **100,** 1071–1078
30. Harris, T. J., and Tepass, U. (2010) Adherens junctions: from molecules to morphogenesis. *Nat. Rev. Mol. Cell Biol.* **11,** 502–514
31. Luo, Y., and Radice, G. L. (2003) Cadherin-mediated adhesion is essential for myofibril continuity across the plasma membrane but not for assembly of the contractile apparatus. *J. Cell Sci.* **116,** 1471–1479
32. Sedarous, M., Keramaris, E., O'Hare, M., Melloni, E., Slack, R. S., Elce, J. S., Greer, P. A., and Park, D. S. (2003) Calpains mediate p53 activation and neuronal death evoked by DNA damage. *J. Biol. Chem.* **278,** 26031–26038
33. Moubarak, R. S., Yuste, V. J., Artus, C., Bouharrour, A., Greer, P. A., Menissier-de Murcia, J., and Susin, S. A. (2007) Sequential activation of poly(ADP-ribose) polymerase 1, calpains, and Bax is essential in apoptosis-inducing factor-mediated programmed necrosis. *Mol. Cell. Biol.* **27,** 4844–4862
34. Chen, M., He, H., Zhan, S., Krajewski, S., Reed, J. C., and Gottlieb, R. A. (2001) Bid is cleaved by calpain to an active fragment *in vitro* and during myocardial ischemia/reperfusion. *J. Biol. Chem.* **276,** 30724–30728
35. Nakagawa, T., and Yuan, J. (2000) Cross-talk between two cysteine protease families. Activation of caspase-12 by calpain in apoptosis. *J. Cell Biol.* **150,** 887–894
36. Polster, B. M., Basañez, G., Etxebarria, A., Hardwick, J. M., and Nicholls, D. G. (2005) Calpain I induces cleavage and release of apoptosis-inducing factor from isolated mitochondria. *J. Biol. Chem.* **280,** 6447–6454
37. Chen, Q., Paillard, M., Gomez, L., Ross, T., Hu, Y., Xu, A., and Lesnefsky, E. J. (2011) Activation of mitochondrial μ-calpain increases AIF cleavage in cardiac mitochondria during ischemia-reperfusion. *Biochem. Biophys. Res. Commun.* **415,** 533–538
38. Artal-Sanz, M., and Tavernarakis, N. (2005) Proteolytic mechanisms in necrotic cell death and neurodegeneration. *FEBS Lett.* **579,** 3287–3296
39. Yousefi, S., Perozzo, R., Schmid, I., Ziemiecki, A., Schaffner, T., Scapozza, L., Brunner, T., and Simon, H. U. (2006) Calpain-mediated cleavage of Atg5 switches autophagy to apoptosis. *Nat. Cell Biol.* **8,** 1124–1132
40. Liu, X., Van Vleet, T., and Schnellmann, R. G. (2004) The role of calpain in oncotic cell death. *Annu. Rev. Pharmacol. Toxicol.* **44,** 349–370
41. Bano, D., Young, K. W., Guerin, C. J., Lefeuvre, R., Rothwell, N. J., Naldini, L., Rizzuto, R., Carafoli, E., and Nicotera, P. (2005) Cleavage of the plasma membrane Na^+/Ca^{2+} exchanger in excitotoxicity. *Cell* **120,** 275–285
42. Ma, J., Wei, M., Wang, Q., Li, J., Wang, H., Liu, W., Lacefield, J. C., Greer, P. A., Karmazyn, M., Fan, G. C., and Peng, T. (2012) Deficiency of Capn4 gene inhibits nuclear factor-κB (NF-κB) protein signaling/inflammation and reduces remodeling after myocardial infarction. *J. Biol. Chem.* **287,** 27480–27489
43. Taneike, M., Mizote, I., Morita, T., Watanabe, T., Hikoso, S., Yamaguchi, O., Takeda, T., Oka, T., Tamai, T., Oyabu, J., Murakawa, T., Nakayama, H., Nishida, K., Takeda, J., Mochizuki, N., Komuro, I., and Otsu, K. (2011) Calpain protects the heart from hemodynamic stress. *J. Biol. Chem.* **286,** 32170–32177
44. Jackson, B. M., Gorman, J. H., Moainie, S. L., Guy, T. S., Narula, N., Narula, J., John-Sutton, M. G., Edmunds, L. H., Jr., and Gorman, R. C. (2002) Extension of borderzone myocardium in postinfarction dilated cardiomyopathy. *J. Am. Coll. Cardiol.* **40,** 1160–1167; discussion 1168–1171
45. Shumway, S. D., Maki, M., and Miyamoto, S. (1999) The PEST domain of IκBα is necessary and sufficient for *in vitro* degradation by μ-calpain. *J. Biol. Chem.* **274,** 30874–30881
46. Sato, N., Fujio, Y., Yamada-Honda, F., Funai, H., Wada, A., Kawashima, S., Awata, N., and Shibata, N. (1995) Elevated calcium level induces calcium-dependent proteolysis of A-CAM (N-cadherin) in heart: analysis by detergent-treated model. *Biochem. Biophys. Res. Commun.* **217,** 649–653
47. Jang, Y. N., Jung, Y. S., Lee, S. H., Moon, C. H., Kim, C. H., and Baik, E. J. (2009) Calpain-mediated N-cadherin proteolytic processing in brain injury. *J. Neurosci.* **29,** 5974–5984
48. Kostetskii, I., Li, J., Xiong, Y., Zhou, R., Ferrari, V. A., Patel, V. V., Molkentin, J. D., and Radice, G. L. (2005) Induced deletion of the N-cadherin gene in the heart leads to dissolution of the intercalated disc structure. *Circ. Res.* **96,** 346–354
49. Matsushita, T., Oyamada, M., Fujimoto, K., Yasuda, Y., Masuda, S., Wada, Y., Oka, T., and Takamatsu, T. (1999) Remodeling of cell-cell and cell-extracellular matrix interactions at the border zone of rat myocardial infarcts. *Circ. Res.* **85,** 1046–1055
50. Wang, X., and Gerdes, A. M. (1999) Chronic pressure overload cardiac hypertrophy and failure in guinea pigs. III. Intercalated disc remodeling. *J. Mol. Cell Cardiol.* **31,** 333–343
51. Schaper, J., Froede, R., Hein, S., Buck, A., Hashizume, H., Speiser, B., Friedl, A., and Bleese, N. (1991) Impairment of the myocardial ultrastructure and changes of the cytoskeleton in dilated cardiomyopathy. *Circulation* **83,** 504–514
52. Dorn, G. W., 2nd. (2009) Novel pharmacotherapies to abrogate postinfarction ventricular remodeling. *Nat. Rev. Cardiol.* **6,** 283–291
53. Letavernier, E., Perez, J., Bellocq, A., Mesnard, L., de Castro Keller, A., Haymann, J. P., and Baud, L. (2008) Targeting the calpain/calpastatin system as a new strategy to prevent cardiovascular remodeling in angiotensin II-induced hypertension. *Circ. Res.* **102,** 720–728
54. Scalia, R., Gong, Y., Berzins, B., Freund, B., Feather, D., Landesberg, G., and Mishra, G. (2011) A novel role for calpain in the endothelial dysfunction induced by activation of angiotensin II type 1 receptor signaling. *Circ. Res.* **108,** 1102–1111

OPEN ACCESS Freely available online

PLOS ONE

N-Glycans: Phenotypic Homology and Structural Differences between Myocardial Cells and Induced Pluripotent Stem Cell-Derived Cardiomyocytes

Takuji Kawamura[1], Shigeru Miyagawa[1], Satsuki Fukushima[1], Akira Yoshida[2], Noriyuki Kashiyama[1], Ai Kawamura[1], Emiko Ito[1], Atsuhiro Saito[1], Akira Maeda[3], Hiroshi Eguchi[3], Koichi Toda[1], Jong-Kook Lee[2], Shuji Miyagawa[3], Yoshiki Sawa[1]*

1 Department of Cardiovascular Surgery, Osaka University Graduate School of Medicine, Suita, Osaka, Japan, **2** Department of Cardiovascular Regenerative Medicine, Osaka University Graduate School of Medicine, Suita, Osaka, Japan, **3** Division of Organ Transplantation, Department of Surgery, Osaka University Graduate School of Medicine, Suita, Osaka, Japan

Abstract

Cell surface glycans vary widely, depending on cell properties. We hypothesized that glycan expression on induced pluripotent stem cells (iPSCs) might change during cardiomyogenic differentiation toward the myocardial phenotype. *N*-glycans were isolated from iPSCs, iPSC-derived cardiomyocytes (iPSC-CM), and original C57BL/6 mouse myocardium (Heart). Their structures were analyzed by a mapping technique based on HPLC elution times and MALDI-TOF/MS spectra. Sixty-eight different *N*-glycans were isolated; the structures of 60 of these *N*-glycans were identified. The quantity of high-mannose type (immature) *N*-glycans on the iPSCs decreased with cardiomyogenic differentiation, but did not reach the low levels observed in the heart. We observed a similar reduction in neutral *N*-glycans and an increase in fucosylated or sialyl *N*-glycans. Some structural differences were detected between iPSC-CM and Heart. No *N*-glycolyl neuraminic acid (NeuGc) structures were detected in iPSC-CM, whereas the heart contained numerous NeuGc structures, corresponding to the expression of cytidine monophosphate-*N*-acetylneuraminic acid hydroxylase. Furthermore, several glycans containing Galα1-6 Gal, rarely identified in the other cells, were detected in the iPSC-CM. The expression of *N*-glycan on murine iPSCs changed toward the myocardial phenotype during cardiomyogenic differentiation, leaving the structural differences of NeuGc content or Galα1-6 Gal structures. Further studies will be warranted to reveal the meaning of the difference of *N*-glycans between the iPSC-CM and the myocardium.

Citation: Kawamura T, Miyagawa S, Fukushima S, Yoshida A, Kashiyama N, et al. (2014) *N*-Glycans: Phenotypic Homology and Structural Differences between Myocardial Cells and Induced Pluripotent Stem Cell-Derived Cardiomyocytes. PLoS ONE 9(10): e111064. doi:10.1371/journal.pone.0111064

Editor: Toru Hosoda, Tokai University, Japan

Received April 30, 2014; **Accepted** September 19, 2014; **Published** October 30, 2014

Data Availability: The authors confirm that all data underlying the findings are fully available without restriction. All relevant data are within the paper and its Supporting Information files.

Funding: YS received the funding to support this work from the Research Center Network for Realization of Regenerative Medicine managed by Centers for Clinical Application Research on Specific Disease/Organ and funded by Japan Science and Technology Agency. The funders had no role in study design, data collection and analysis, decision to publish, or preparation of the manuscript.

Competing Interests: The authors have declared that no competing interests exist.

* Email: sawa-p@surg1.med.osaka-u.ac.jp

Introduction

In vitro generation of cardiac myocytes by reprogramming is a promising technology in developing cell-transplant therapy for advanced cardiac failure [1] and drug discovery for a variety of cardiac diseases [2]. For both purposes, induced pluripotent stem cells (iPSCs) are most useful, since generation and cardiomyogenic differentiation of iPSCs has been standardized in human and a number of animals [3,4]. In fact, derivatives of iPSCs have been developed to the pre-clinical stage for cell transplantation therapy [5], while cardiac myocytes generated from patient-specific iPSCs have been studied to explore pathologic mechanisms and guide drug discovery [6,7]. However, cardiac myocyte preparations from iPSCs contain immature phenotypes, observed by electrophysiology, electron microscopy, and immunohistochemistry [8,9]; this may limit the safety and efficacy of cell transplantation therapy or reduce the accuracy and efficiency of drug discovery. The maturity of iPSC-derived cardiac myocytes (iPSC-CMs) has not been comprehensively or quantitatively evaluated.

Cell surface glycans have several important functions interacting with numerous proteins, including growth factors, morphogens and adhesion molecules, modulating dynamic cellular mechanisms such as cell-cell adhesion, cell activation, and malignant alterations [10–12]. In early mammalian embryos, associated with fertilization, some *N*-glycans play important roles of cell-cell adhesion [13–15]. In addition, cellular responsiveness to growth or arrest depends on total *N*-glycan number and the degree of branching of cell surface glycoproteins [16]. Furthermore, heparan sulfate, a kind of glycans, is required for embryonic stem cell (ESC) pluripotency, in particular lineage specification into mesoderm through facilitation of FGF and BMP signaling by stabilizing BMP ligand [17], leading the evidence that the expression patterns of cell surface glycans on ESCs changes during differentiation [18]. Thus, we hypothesized that cell surface glycan expression may

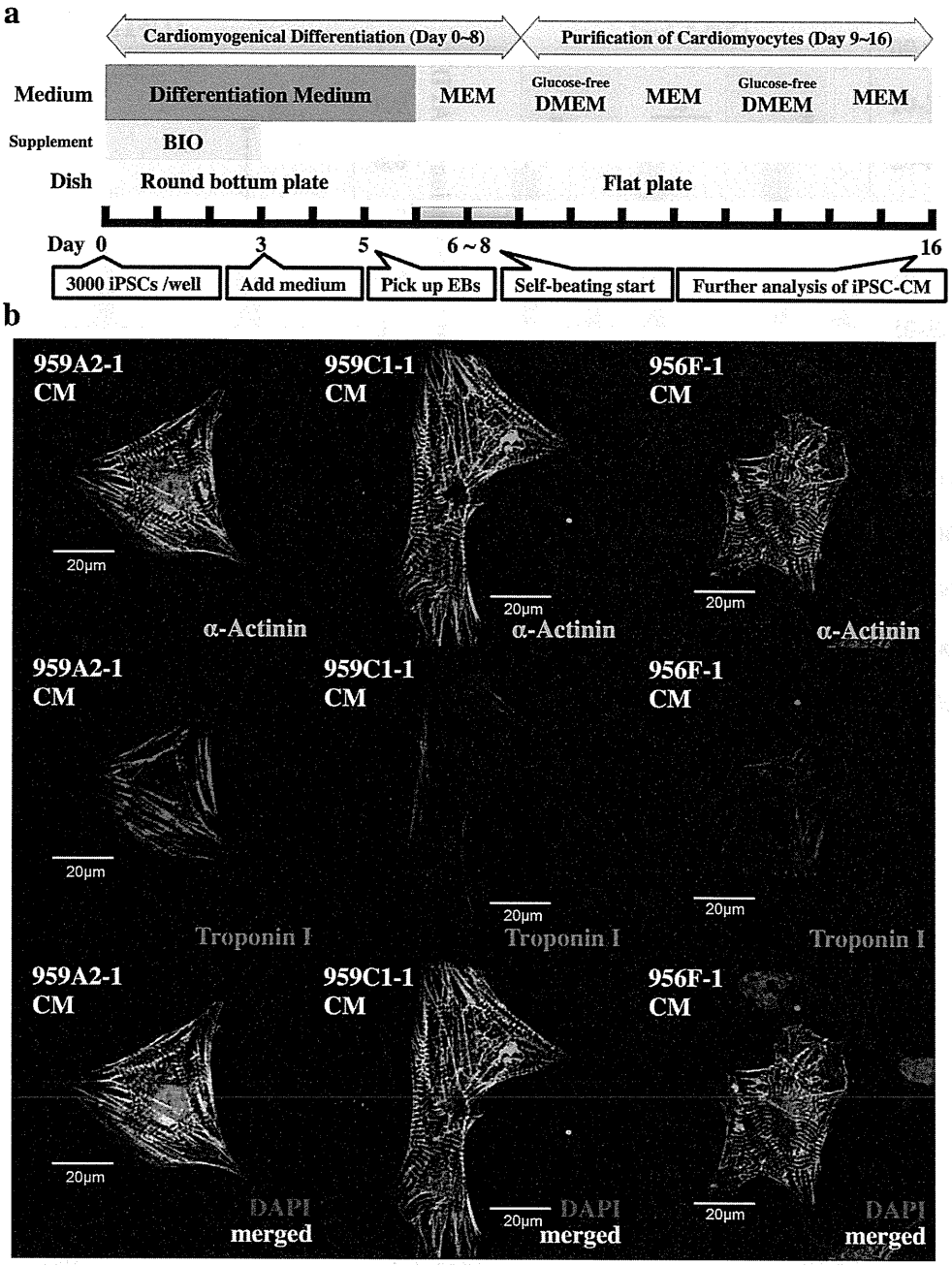

Figure 1. Cardiomyogenic differentiation of iPSCs and cardiomyocyte purification. (a) The cardiomyogenic differentiation protocol and cardiomyocyte purification process are illustrated. (b) IPSC-CMs stained with anti-α-actinin antibody (Alexa Fluor 488), anti-troponin I (Alexa Fluor 594) and DAPI, were analyzed with a confocal laser scanning microscopy. Abbreviations: EB, embryonic body; MEM, Modified Eagle's Medium; DMEM, Dulbecco's Modified Eagle's Medium; BIO, 6-bromoindirubin-3′-oxime.
doi:10.1371/journal.pone.0111064.g001

change during the course of cardiomyogenic differentiation of iPSCs *in vitro*. We analyzed *N*-glycan expression in undifferentiated iPSCs, iPSC-CMs, and adult murine myocardium by HPLC, to identify potential indicators of the maturity of differentiating cardiomyocytes from iPS cells *in vitro*.

Materials and Methods

Animal care procedures were consistent with the "Guide for the Care and Use of Laboratory Animals" (National Institutes of Health publication). Experimental protocols were approved by the

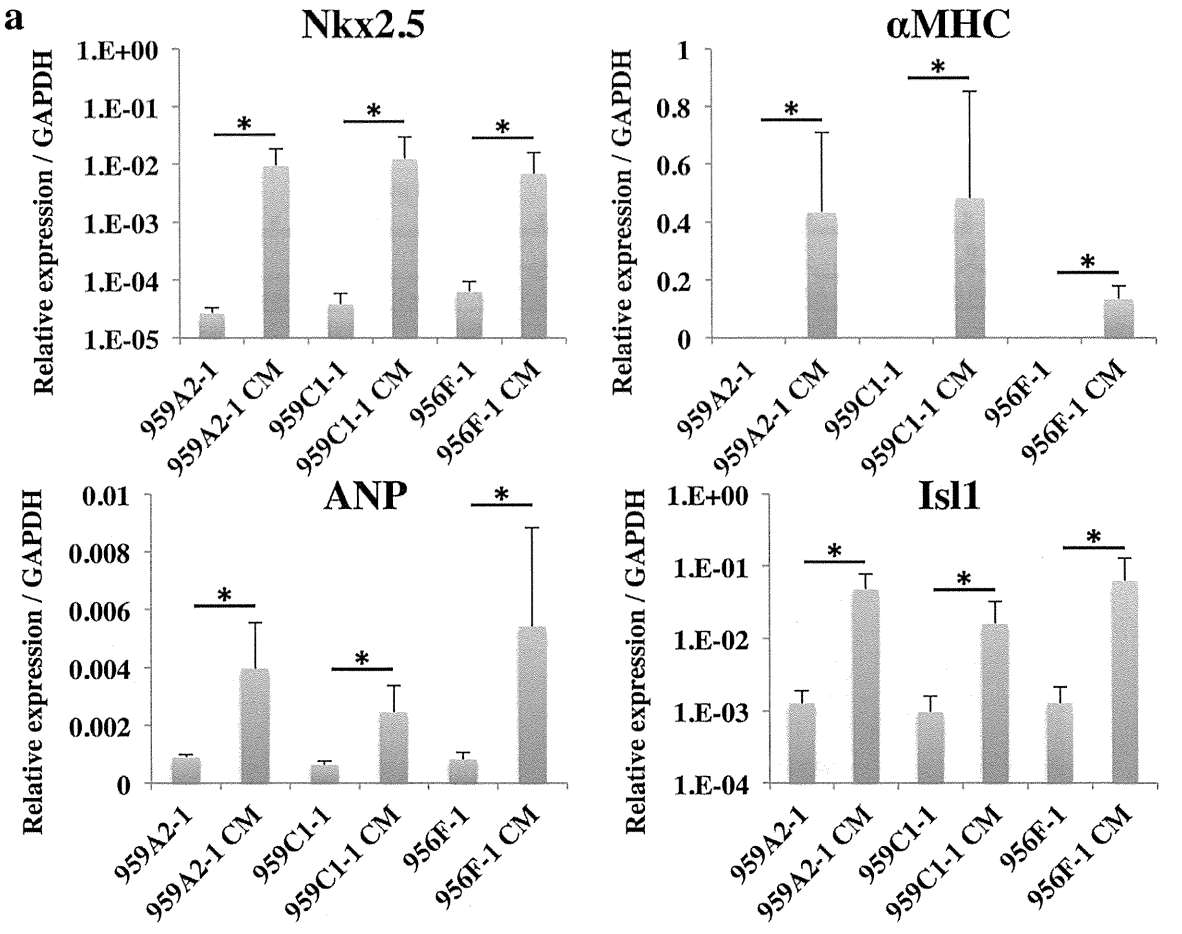
a
Nkx2.5
αMHC
ANP
Isl1
Relative expression / GAPDH
959A2-1
959A2-1 CM
959C1-1
959C1-1 CM
956F-1
956F-1 CM

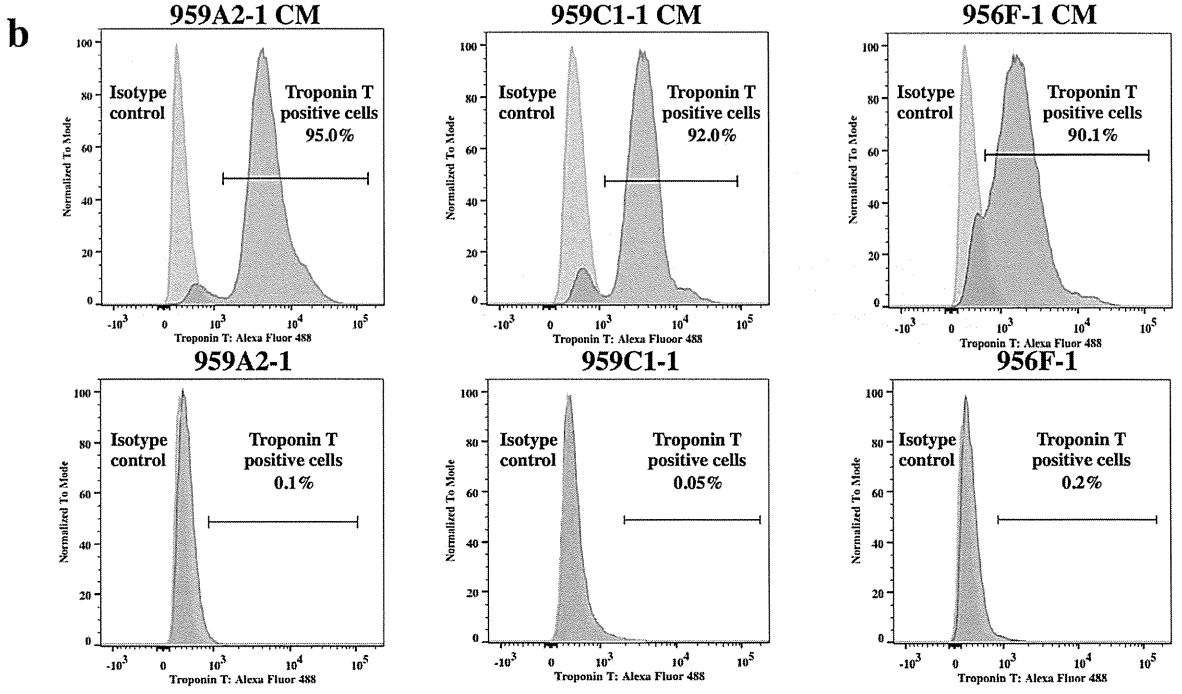
b
959A2-1 CM
959C1-1 CM
956F-1 CM
959A2-1
959C1-1
956F-1
Isotype control
Troponin T positive cells
95.0%
92.0%
90.1%
0.1%
0.05%
0.2%
Normalized To Mode
Troponin T: Alexa Fluor 488

Figure 2. Highly purified iPSC-CMs expressing cardiomyocyte marker genes. (a) Transcript expression of Nkx2.5, αMHC, ANP and Isl1 in the iPSCs and the iPSC-CMs were analyzed by real-time PCR. Results are expressed as the mean ± standard deviation. *P<0.05. (b) IPSC-CMs and iPSCs stained with anti-troponin T antibody or the isotype control, followed by Alexa Fluor 488-conjugated anti-mouse IgG antibody, were analyzed by flow cytometry.
doi:10.1371/journal.pone.0111064.g002

Ethics Review Committee for Animal Experimentation of Osaka University Graduate School of Medicine.

Cardiomyogenic differentiation of murine iPSCs *in vitro*

We used the murine iPSC lines, 959A2-1, 959C1-1, 956F-1 (generous gifts from Dr. Okita and Professor Yamanaka of the Center for iPS Cell Research and Application, Kyoto University, Kyoto, Japan). The cell lines were generated from C57BL/6 (B6) (CLEA) mouse embryonic fibroblasts by introducing *Oct3/4, Sox2, Klf4*, and *c-Myc* without viral vectors as described [19]. The iPSCs were cultured in the absence of serum and feeder cells by using ESGRO Complete PLUS Clonal Grade Medium (Millipore).

Cardiomyogenic differentiation of the iPSCs was performed as described [20,21], with modifications, followed by purification with glucose-free medium supplemented with lactic acid [22]; iPSCs (3×10^3) were resuspended in 100-μL aliquots of differentiation medium [DM; Dulbecco's Modified Eagle's Medium (DMEM; Nacalai Tesque) containing 15% fetal bovine serum (FBS; Biofill), 100 μmol/L non-essential amino acids (NEAA; Invitrogen), 2 mmol/L L-glutamine (Invitrogen), and 0.1 mmol/L 2-mercaptoethanol (Invitrogen)] containing 0.2 μmol/L 6-bromoindirubin-3′-oxime (BIO; a glycogen synthase kinase-3β inhibitor, to activate the Wnt-signaling pathway) (Calbiochem), and cultured in 96-well Corning Costar Ultra-Low attachment multiwell plates (Sigma-Aldrich) for 3 days. On day 3, an additional 100 μL DM without BIO was added to each well. On day 5, individual embryoid bodies (EBs) were transferred to 100-mm gelatin-coated dishes (250 EBs per dish). On days 6, 7, 10, 11, 14, and 15 the medium was exchanged for serum-free Modified Eagle's Medium (MEM; Invitrogen) with insulin transferrin-selenium-X (Invitrogen). On days 8, 9, 12, and 13, the medium was exchanged for Glucose-free DMEM (no glucose, no pyruvate, Invitrogen) supplemented with 4 mmol/L lactic acid (Wako Pure Chemical) for purification of cardiomyocytes. On day 16, the contracting cell clusters were used as cardiomyogenically differentiated iPSCs (959A2-1 CMs, 959C1-1 CMs, 956F-1 CMs: iPSC-CMs). The protocol and purification process are illustrated in Figure 1a.

Adult cardiac tissue from B6 mice (CLEA) was used as a control. Male B6 mice (8 weeks old) were sacrificed by intravenous administration of potassium chloride under inhalation anesthesia of isoflurane, and heart tissue from the left ventricle was harvested for further studies and labeled "Heart".

Immunohistochemistry analysis

IPSC-CMs were dissociated with 0.25% trypsin-EDTA and then fixed with 4% paraformaldehyde. The cells were stained with the following primary antibodies: mouse anti-α-actinin antibody (Sigma-Aldrich) and rabbit anti-troponin I antibody (Abcam), and then visualized by the following secondary antibodies: Alexa Fluor 488 donkey anti-mouse IgG (Invitrogen) and Alexa Fluor 594 goat anti-rabbit IgG (Invitrogen). The nucleus of the cells were stained with 4′, 6-Diamidino-2-phenylindole dihydrochloride (DAPI) and then observed with a confocal laser scanning microscopy FV1200 (Olympus).

Ca^{2+} transient measurement and pharmacological analysis

5 μM Fluo-8 regents (AAT Bioquest, Inc.) in serum-free MEM was added to iPSC-CMs after the cells were washed with phosphate buffered saline. The cells were incubated at 37°C for 30 min and then observed with a fluorescence microscopy. Fluorescence intensity of Fluo-8 dye was sequentially measured using iQ2 software (ANDOR) pre and post the administration of 1 μM isoproterenol.

Flow cytometry

IPSC-CMs were dissociated with 0.25% trypsin-EDTA and then fixed with CytoFix fixation buffer (BD) for 20 min. The cells were permeabilized with Perm/Wash buffer (BD) at room temperature for 10 min and then incubated with mouse anti-troponin T antibody (Thermo) for 30 min. Cells were washed with Perm/Wash buffer prior to incubation with the Alexa Fluor 488 rabbit anti-mouse IgG secondary antibody (Invitrogen) at room temperature for 30 min. These cells were analyzed on a FACS Canto II (BD).

Characterization of *N*-glycans derived from iPSCs, iPSC-CM, and Heart

All experimental procedures, including chromatography conditions and glycosidase treatments, have been described previously [23]. Cultured undifferentiated iPSCs, iPSC-CMs, and the heart tissue were treated with chloroform–methanol, then subjected to proteolysis with chymotrypsin and trypsin, followed by glycoamidase A digestion to release *N*-glycans. After removal of peptides, the reducing ends of the *N*-glycans were derivatized with 2-aminopyridine (Wako). This mixture was applied to a diethylaminoethyl (DEAE) column (Tosoh) or a TSK-gel Amide-80 column (Tosoh); each fraction from the amide column was then applied to a Shim-pack HRC-octadecyl silane (ODS) column (Shimadzu). The elution times of individual peaks from the amide-silica and ODS columns were normalized to a pyridylamino (PA)-derivatized isomalto-oligosaccharide with a known degree of polymerization, and are represented as glucose units (GU). Thus, each compound from these two columns provided a unique set of GU values, which corresponded to the coordinates of the 2D HPLC map. The PA-oligosaccharides were identified by comparison to the coordinates of ~500 reference PA-oligosaccharides in a homemade web application, GALAXY (http://www.glycoanalysis.info/galaxy2/ENG/index.jsp) [24]. The calculated HPLC map based on the unit contribution values was used to estimate some high-mannose type PA-oligosaccharides. The PA-oligosaccharides were co-chromatographed with the reference to PA-oligosaccharides on the columns to confirm their identities. PA-glycans that did not correspond to any of the *N*-glycans registered in GALAXY were trimmed by exoglycosidase to produce a series of known glycans [25].

Mass spectrometry

PA-oligosaccharides were analyzed by matrix-assisted laser desorption/ionization time-of-flight mass spectrometric (MALDI-TOF/MS). The matrix solution was prepared as follows: 10 mg of 2,5-Dihydroxybenzoic acid (Sigma) was dissolved in 1:1 (v/v)

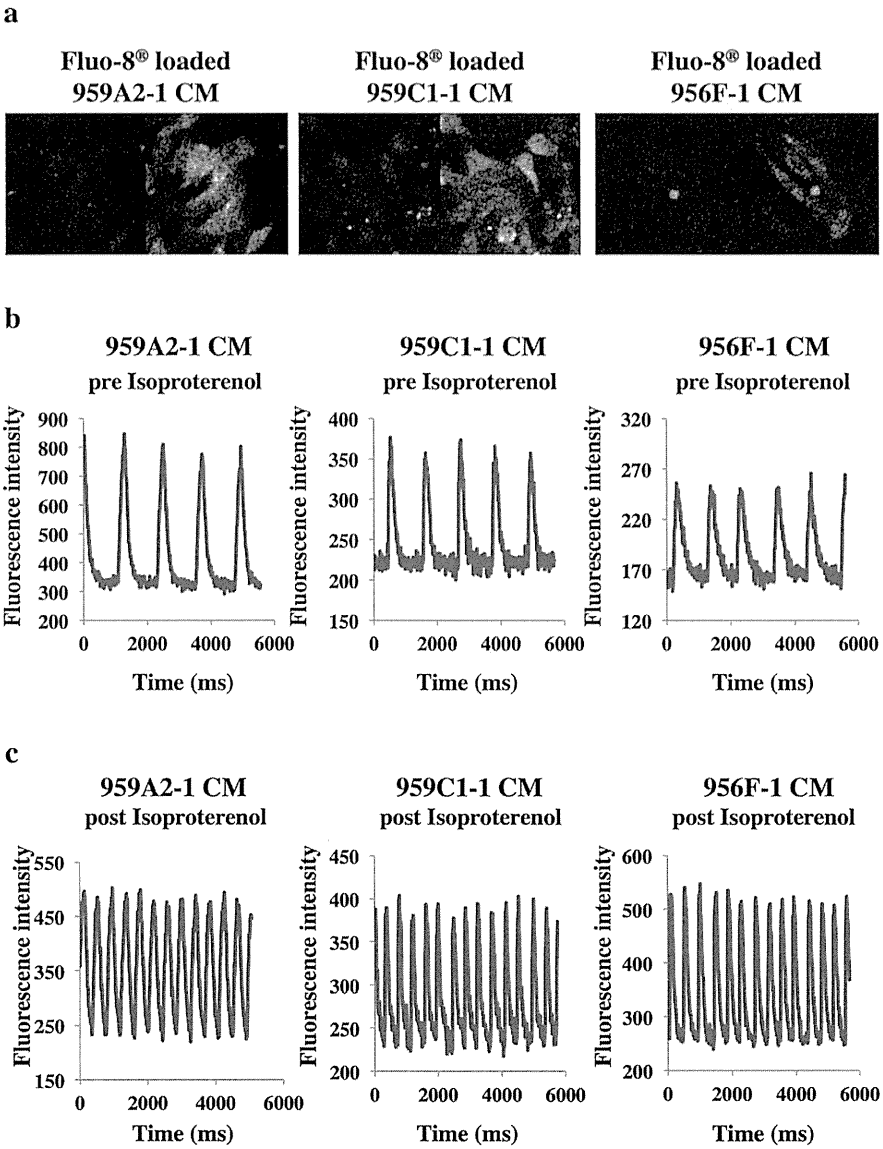

Figure 3. Ca^{2+} transient measurement of iPSC-CMs pre and post the administration of isoproterenol. (a) Fluo-8 loaded iPSC-CMs at the time of low (left) and high (right) fluorescence. (b), (c) Sequentially measured fluorescence intensity of Fluo-8 loaded iPSC-CMs pre (b) and post (c) the administration of 1 μM isoproterenol.
doi:10.1371/journal.pone.0111064.g003

acetonitrile/water (1 mL). Stock solutions of PA-glycans were prepared by dissolving them in pure water. One microliter of a sample solution was mixed on the target spot of a plate with 1 μL matrix solution and then allowed to air-dry. MALDI-TOF/MS data were acquired in the positive mode on an AXIMA-CFR (Shimadzu) operated in linear mode.

Materials

Glycoamidase A from sweet almond, α-mannosidase, β-galactosidase, and β-*N*-acetylhexosaminidase from jack bean were purchased from Seikagaku Kogyo (Tokyo, Japan). α-Galactosidase from coffee bean was purchased from Oxford GlycoSciences (Oxford, UK). Trypsin and chymotrypsin were obtained from Sigma (St. Louis, MO). Pronase protease from *Streptomyces griseus* was from Calbiochem (San Diego, CA). The pyridylamino (PA) derivatives of isomalto-oligosaccharides 4–20 (indicating the degree of polymerization of glucose residues) and reference PA-oligosaccharides were purchased from Seikagaku Kogyo.

Semi-quantitative PCR

DNA-free total RNA was extracted with the RNeasy RNA isolation Kit (Qiagen) and reverse-transcribed into cDNA using Omniscript reverse transcriptase (Qiagen), then analyzed by quantitative real-time PCR on an ABI PRISM 7700 thermocycler (Applied Biosystems) with the following TaqMan gene expression assays (Applied Biosystems): ST3Gal-III (Gal β1-3(4) GlcNAc α-2,

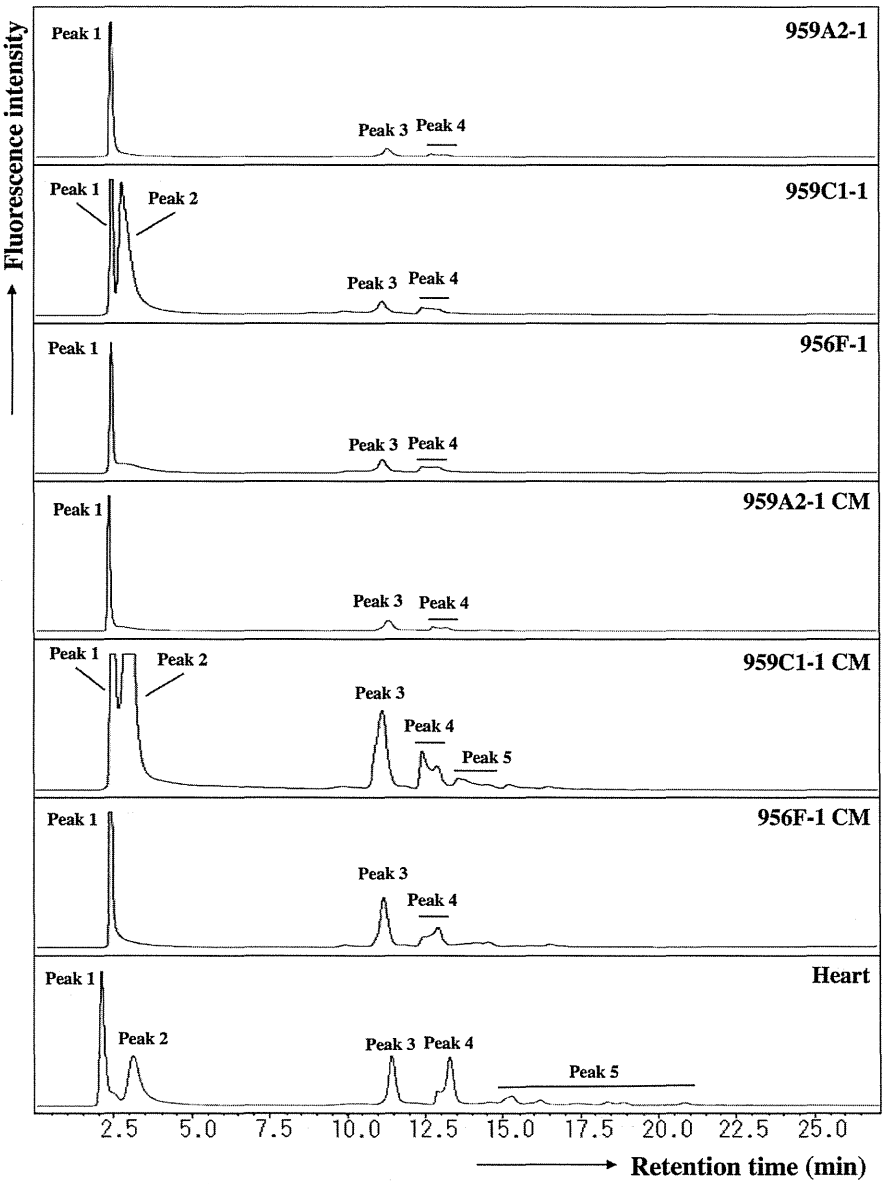

Figure 4. Anion-exchange DEAE elution profiles of PA-glycans. PA-glycans were fractionated according to their sialic acid content as neutral (peak 1), monosialyl (peak 3), and disialyl (peak 4) oligosaccharide fractions. Peaks 2 and 5 represent fractions containing no detectable PA-oligosaccharides.
doi:10.1371/journal.pone.0111064.g004

3-sialyltransferase), Mm00493353_m1; ST4Gal-IV (Gal β1-4(3) GlcNAc α-2, 3-sialyltransferase), Mm00501503_m1; ST6Gal-I (Gal β1-4 GlcNAc α-2, 6-sialyltransferase), Mm00486119_m1; CMAH (cytidine monophosphate-*N*-acetylneuraminic acid hydroxylase), Mm00483341_m1; GAPDH (glyceraldehyde-3-phosphate dehydrogenase), and Mm03302249_g1 and with SYBR Green dye (Applied Biosystems) using the following primers: Nkx2.5 F, 5′- CAAGTGCTCTCCTGCTTTCC -3′ R, 5′- GGCTTTGTCCAGCTCCACT -3′; αMHC (α-myosin heavy chain) F, 5′- GAGATTTCTCCAACCCAG -3′ R, 5′- TCTGACTTTCGGAGGTACT-3′; ANP (atrial natriuretic peptide) F, 5′-AAAGAAACCAGAGTGGGCAGAG -3′ R, 5′- CCAGGGTGATGGAGAAGGAG -3′; Isl1 F, 5′- TTTCCCTGTGTGTTGGTTGC -3′ R, 5′- TGATTACACTCCGCACATTTCA -3′; GAPDH F, 5′- CCAGTATGACTCCACTCACG -3′ R, 5′- GACTCCACGACATACTCAGC -3′. All experiments were performed by the relative standard curve method in three independent, triplicate experiments. Statistical comparison of the data was performed by Student's t-test.

Results

Highly purified cardiomyocytes derived from iPSCs

Cardiomyogenic differentiation was induced in murine iPSCs by using a slightly modified culture protocol (Figure 1a). The iPSC-CMs showed significantly higher expressions of Nkx2.5,

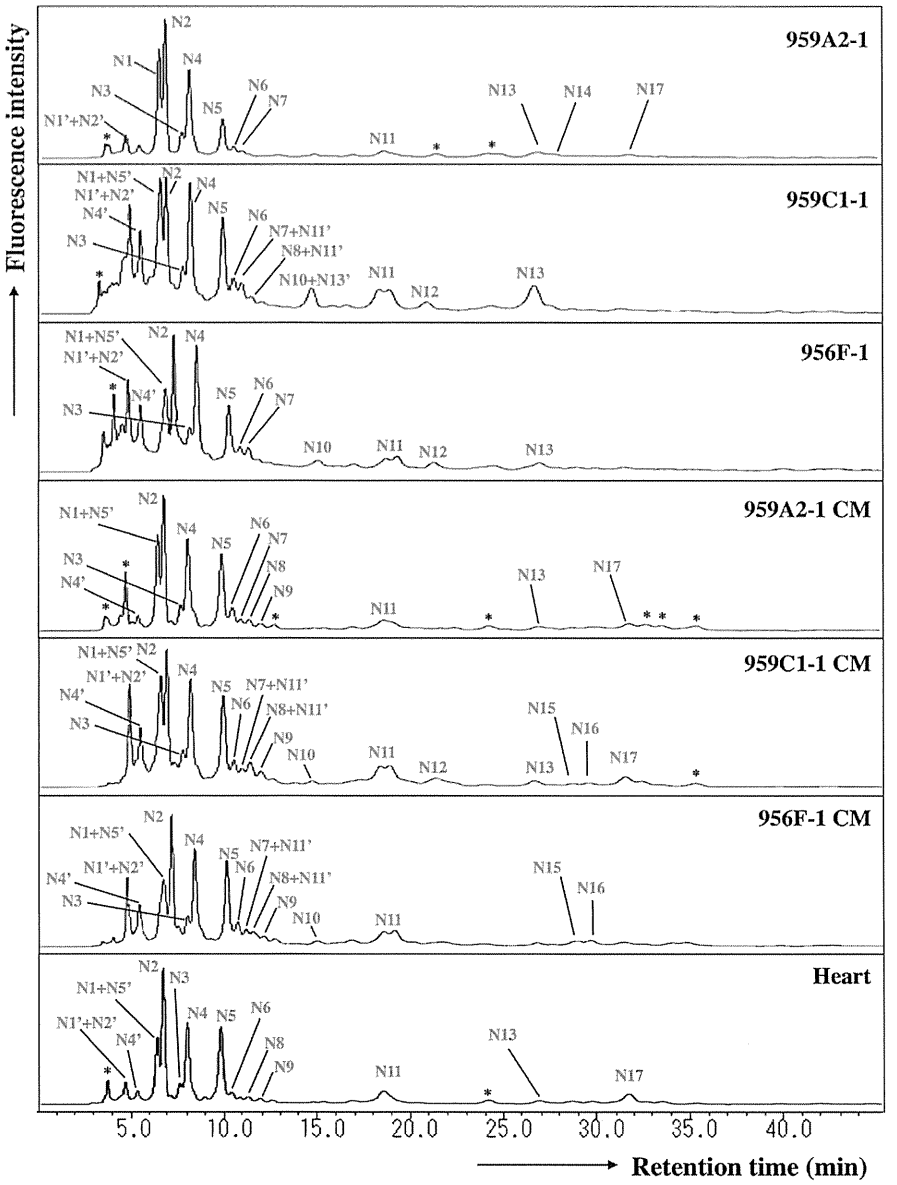

Figure 5. Reverse-phase ODS elution profiles of the neutral PA-glycans. The neutral fractions were individually applied to the ODS column and eluted according to their hydrophobicity. N1′, N2′, N4′, N5′ and N11′: epimerization of N1, N2, N4, N5 and N11. *Fractions containing no detectable PA-oligosaccharides.
doi:10.1371/journal.pone.0111064.g005

αMHC, ANP and Isl1 than undifferentiated iPSCs by semi-quantitative real-time PCR (Figure 2a), and showed sarcomere structures observed by immunohistological staining of α-actinin and troponin I (Figure 1b). The iPSC-CMs were functional with Ca^{2+} transient measurement (Figure 3a, b) and their beating rates were increased by the administration of isoproterenol (Figure 3c), meaning they had β-adrenergic receptors. Nearly all of the iPSC-CMs exhibited spontaneous and regular beating at room temperature (Video S1). The differentiation efficiency of murine iPSC was evaluated by flow cytometry analysis. More than 95% of the 959A2-1 CMs, 92% of the 959C1-1 CMs and 90% of the 956F-1 CMs were positive for troponin T (Figure 2b), while the undifferentiated iPSCs rarely expressed troponin T (Figure 2b).

N-Glycans isolated from iPSCs, iPSC-CM, and Heart

N-glycans extracted from undifferentiated iPSCs (959A2-1: 26 mg, 959C1-1: 11 mg and 956F-1: 10 mg of protein), iPSC-CM (959A2-1 CM: 15 mg, 959C1-1 CM: 12 mg and 956F-1 CM: 5.5 mg of protein), and the B6 heart muscle (82 mg of protein) were separated on a diethylaminoethyl (DEAE) column into five peaks, based on increasing acidity. Peak 1 represented a neutral (N) fraction, peak 3 a monosialyl (M) fraction, and peak 4 a disialyl

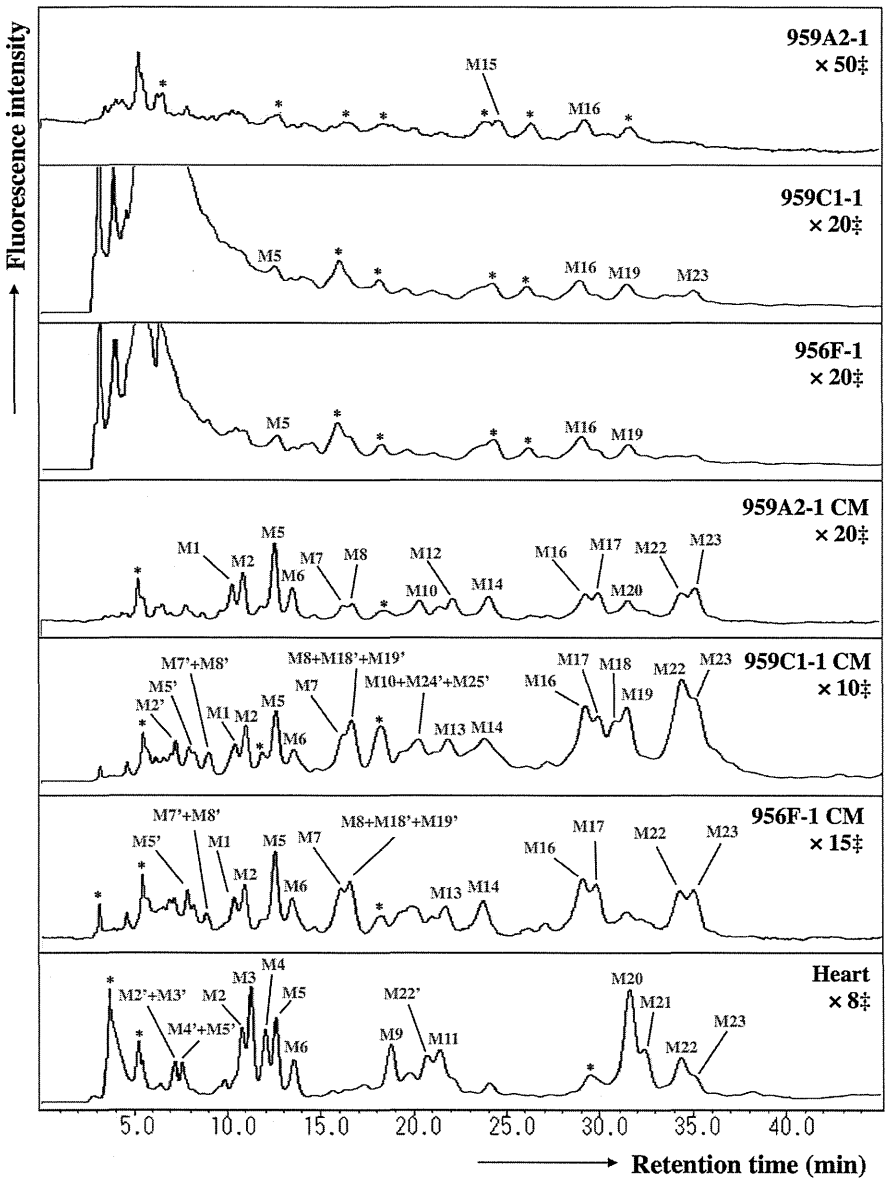

Figure 6. Reverse-phase ODS elution profiles of monosialyl PA-glycans. The monosialyl fractions were individually applied to the ODS column and eluted according to their hydrophobicity. M2′, M3′, M4′, M5′, M7′, M8′, M18′, M19′, M22′, M24′ and M25′: epimerization of M2, M3, M4, M5, M7, M8, M18, M19, M22, M24 and M25. *Fractions containing no detectable PA-oligosaccharides. ‡Magnification ratio to the fluorescence intensity of asialoglycan of each sample.
doi:10.1371/journal.pone.0111064.g006

(D) fraction. Glycan fractions in each of these peaks were as follows: iPSCs yielded 97% N, 0.5% M, 2.6% D (959A2-1), 98% N, 0.7% M, 1.1% D (959C1-1) and 96% N, 1.1% M, 3.1% D (956F-1) peak areas, iPSC-CMs yielded 89% N, 6.4% M, 4.4% D (959A2-1 CM), 79% N, 16% M, 4.8% D (959C1-1 CM) and 82% N, 10% M, 7.9% D (956F-1 CM) and Heart yielded 55% N, 19% M, and 25% D (Figure 4).

The ODS column separated the neutral fraction (Peak 1) into fractions N1–N17 (Figure 5), the monosialyl fraction (Peak 3) into fractions M1–M23 (Figure 6), and the disialyl fraction (Peak 4) into fractions D1–D12 (Figure 7). The signatures of each fraction differed between groups. These ODS fractions were individually fractionated on an amide column and analyzed by MALDI-TOF/MS. The N2, M6, M11, M14, M20, D4, D5, and D10 fractions contained two types of *N*-glycans, and the N6, N9, N11 and M2 fractions three types (data not shown). Thus, 68 different *N*-glycans were isolated from iPSCs, iPSC-CMs, and Heart.

Structures of *N*-Glycans isolated from iPSCs, iPSC-CM, and Heart

The isolated *N*-glycans were analyzed by means of a mapping technique based on their HPLC elution positions and MALDI-TOF/

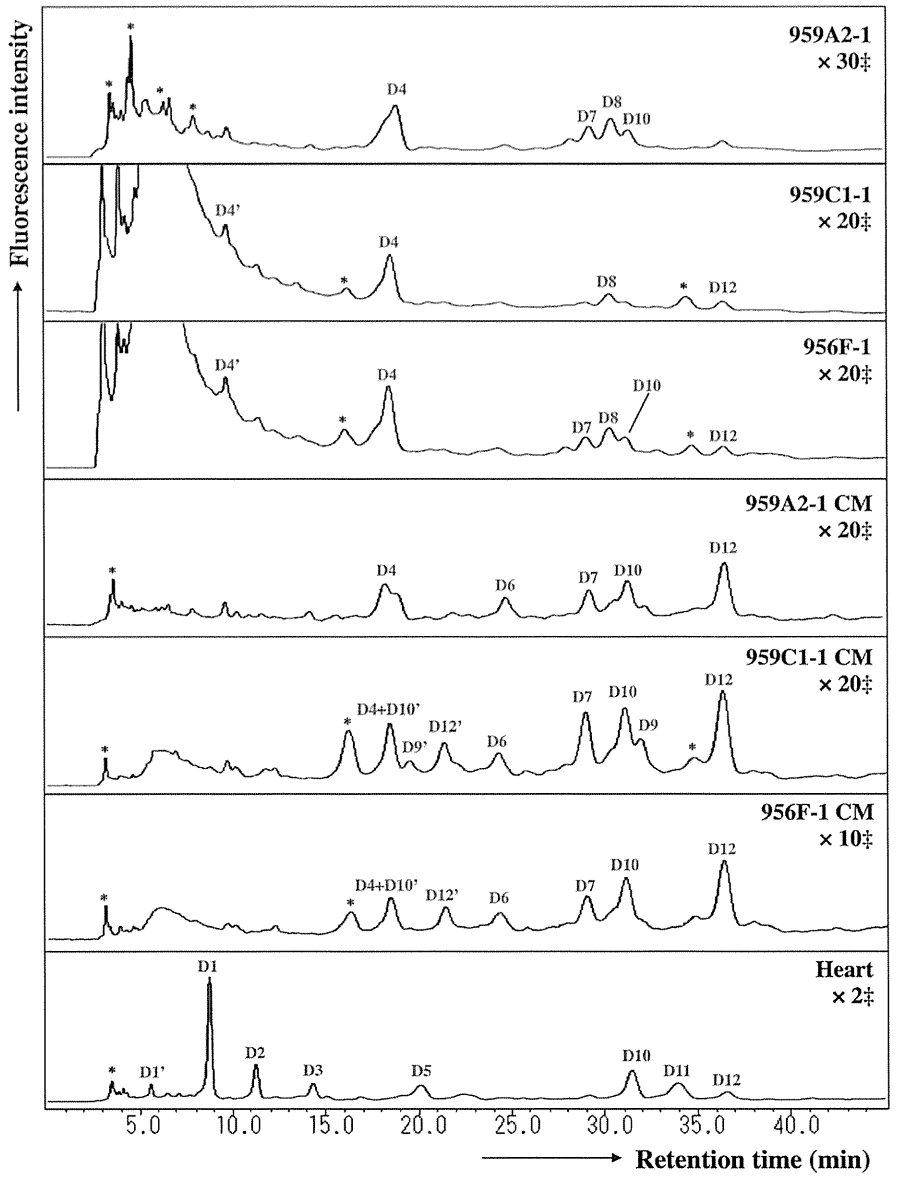

Figure 7. Reverse-phase ODS elution profiles of disialyl PA-glycans. The disialyl fractions were individually applied to the ODS column and eluted according to their hydrophobicity. D1′, D4′, D10′ and D12′: epimerization of D1, D4, D10 and D12; *Fractions containing no detectable PA-oligosaccharides. ‡Magnification ratio to the fluorescence intensity of asialoglycan of each sample.
doi:10.1371/journal.pone.0111064.g007

MS data. The coordinates of 54 *N*-glycans coincided with those for known references in the GALAXY database and their structures were identified. The coordinates for N9-3, M8, M11-2, M12, M13, M15, M17, M18, M19, M20-2, M21, M23, D8 and D9 did not correspond to known references.

N-glycans N9-2, M8, M12, M17, and M23 were trimmed by α-galactosidase but not by β-galactosidase or *N*-acetylglucosamidase. Their structures fit GALAXY references H5.12, 1A1-200.4, 1A3-200.4, 1A1-210.4, and 1A3-210.4, respectively. The galactosyl structures were then identified as Galα1-6Gal, because of the α-galactosidase-driven MS shifts. The structure of the M13 was identified by the coincidence with a GALAXY reference 1A2-H5.12 after being trimmed by α-L-fucosidase. The other *N*-glycans M11-2, M15, M18, M19, M20-2, M21, D8 and D9 were not identified in this study because they did not correspond to GALAXY references even after α-galactosidase digestions. They are described in Figure 8 and Table S1-S5 with their proposed formulas based on MALDI-TOF/MS data.

High-mannose *N*-Glycans were reduced by cardiomyogenic differentiation

The quantity of high-mannose *N*-glycans (HM) calculated from the total volume of N1–N6-2, N7 was highest in the iPSCs (959A2-1: 87.7%, 959C1-1: 68.3% and 956F-1: 78.2%), lower in the

Code No.	N1	N2-1	N2-2	N3	N4	N5	N6-1	N6-2	N6-3	N7	N8	N9-1
GU; ODS (Amid)	5.0 (8.8)	5.3 (7.9)	5.3 (9.5)	6.0 (7.8)	6.2 (7.0)	7.3 (6.0)	7.6 (4.2)	7.6 (5.0)	7.6 (4.6)	7.9 (3.3)	8.1 (7.3)	8.2 (5.6)
Mass (Da)	1800	1638	1962	1638	1475	1313	989	1151	1192	827	1679	1354
Structure	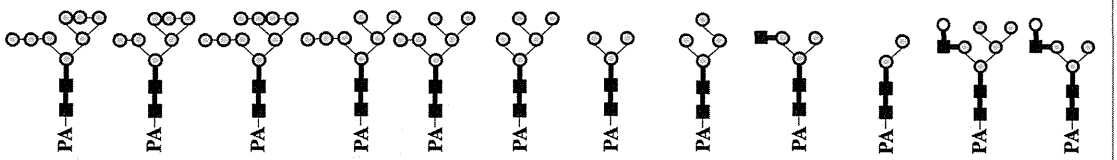											

N9-2	N9-3	N10	N11-1	N11-2	N11-3	N12	N13	N14	N15	N16	N17
8.2 (6.4)	8.3 (8.2)	9.3 (5.0)	10.5 (3.7)	10.5 (4.6)	10.5 (6.9)	11.2 (6.1)	12.8 (5.3)	13.0 (5.0)	13.3 (6.2)	13.5 (6.3)	14.2 (7.3)
1516	1841	1395	973	1135	1720	1500	1541	1338	1704	1704	1866
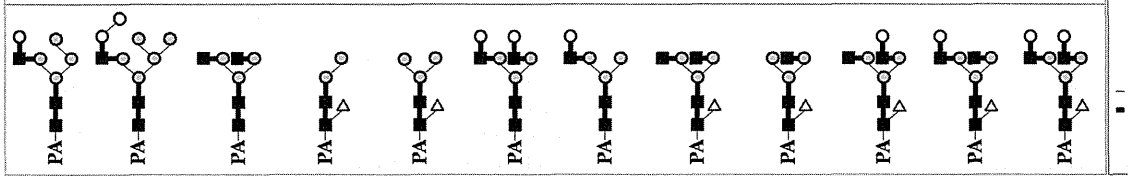											

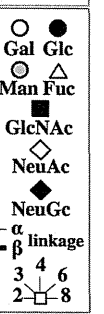

M1	M2-1	M2-2	M2-3	M3	M4	M5	M6-1	M6-2	M7	M8	M9	M10	M11-1	M11-2
7.6 (7.5)	7.9 (5.8)	7.9 (6.6)	7.9 (7.5)	8.1 (7.5)	8.4 (6.7)	8.6 (7.0)	9.0 (5.3)	9.0 (6.1)	10.1 (7.1)	10.3 (7.9)	10.6 (7.1)	11.0 (6.3)	11.3 (6.6)	11.3 (8.8)
1970	1646	1808	2027	1986	1824	1970	1646	1808	2011	2173	2027	1792	2011	2360
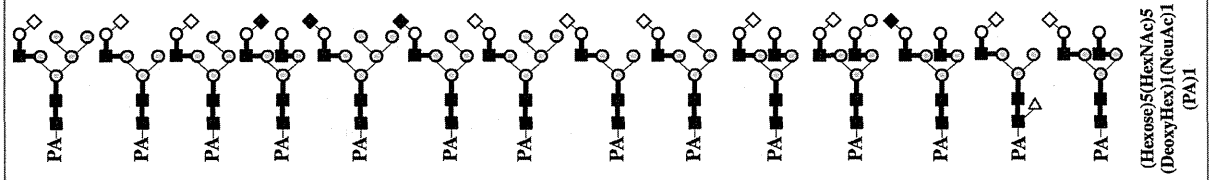														

M12	M13	M14-1	M14-2	M15	M16	M17	M18	M19	M20-1	M20-2	M21	M22	M23
11.5 (7.4)	11.3 (7.4)	11.8 (6.5)	11.8 (5.6)	12.1 (8.3)	13.3 (7.5)	13.7 (8.3)	13.8 (7.4)	14.0 (8.2)	14.2 (7.5)	14.2 (8.2)	14.5 (8.3)	15.1 (6.9)	15.3 (7.8)
2173	2116	1954	1792	2173	2157	2320	2360	2522	2173	2522	2344	2157	2320
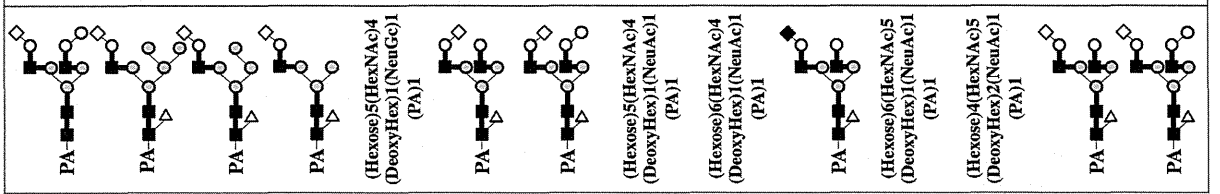													

D1	D2	D3	D4-1	D4-2	D5-1	D5-2	D6	D7	D8	D9	D10-1	D10-2	D11	D12
7.0 (8.2)	8.3 (7.8)	9.3 (8.6)	10.6 (6.9)	10.6 (7.3)	10.9 (7.4)	10.9 (8.1)	12.1 (6.4)	13.5 (7.7)	13.9 (6.8)	14.1 (7.5)	14.2 (7.2)	14.2 (7.7)	15.0 (7.2)	15.9 (6.7)
2334	2334	2480	2302	2302	2334	2480	2302	2448	2537	2854	2448	2480	2464	2448